General Disclaimer

One or more of the Following Statements may affect this Document

- This document has been reproduced from the best copy furnished by the organizational source. It is being released in the interest of making available as much information as possible.

- This document may contain data, which exceeds the sheet parameters. It was furnished in this condition by the organizational source and is the best copy available.

- This document may contain tone-on-tone or color graphs, charts and/or pictures, which have been reproduced in black and white.

- This document is paginated as submitted by the original source.

- Portions of this document are not fully legible due to the historical nature of some of the material. However, it is the best reproduction available from the original submission.

1321-F-2

NASA/HOE

DRA

FINAL REPORT

HOLOGRAPHIC OPTICAL ELEMENTS: FABRICATION AND TESTING

PREPARED FOR

NATIONAL AERONAUTICS AND SPACE ADMINISTRATION

GEORGE C. MARSHALL SPACE FLIGHT CENTER

CONTRACT NO. NAS8-28949

MARCH 1974

BY

ELECTRO-OPTICS OPERATION

RADIATION

A DIVISION OF HARRIS-INTERTYPE CORPORATION

87974

1321-F-2

NASA/HOE

FINAL REPORT

HOLOGRAPHIC OPTICAL ELEMENTS: FABRICATION AND TESTING

PREPARED FOR

NATIONAL AERONAUTICS AND SPACE ADMINISTRATION

GEORGE C. MARSHALL SPACE FLIGHT CENTER

CONTRACT NO. NAS8-28949

MARCH 1974

BY

ELECTRO-OPTICS OPERATION

FOREWARD

This report was prepared by the Electro-Optics Operation of Radiation, a Division of Harris-Intertype Corporation, and covers the work performed between July 1973 and March 1974 on Contract Number NAS 8-28949. The effort is monitored by Mr. E. J. Reinbolt. The contractor's report number is 1321-F-2.

The principal investigators for the program are R. G. Zech, M. Shareck and L. M. Ralston. The Program Manager is R. G. Zech. Contributors to this report are W. Colburn*, Dr. A. A. Friesem, Dr. W. H. Lee, L. M. Ralston, M. Shareck and R. G. Zech. This report was prepared under the general direction of Dr. A. Vander Lugt, Director, Systems and Programs Group.

* Radar and Optics Group, Environmental Research Institute of Michigan, Ann Arbor, Michigan.

TABLE OF CONTENTS

TABLE OF CONTENTS... Continued

LIST OF ILLUSTRATIONS

LIST OF ILLUSTRATIONS... Continued

LIST OF ILLUSTRATIONS... Continued

LIST OF TABLES

SECTION 1
INTRODUCTION

1.0 INTRODUCTION

This report completes the second phase of a comprehensive program designed to investigate the basic properties of holographic optical systems. In review, the first phase of the program produced the following important contributions to the field of holographic optics:

- An indepth experimental study of single element holographic optics.
- A verification of the accuracy of the analytical and computer-based description of hologram behavior.
- An evaluation of candidate hologram recording materials.
- A preliminary investigation of multielement holographic optical systems.

To obtain these advances, we performed an extensive analytic and experimental study. Using interferometric methods we measured both chromatic and Seidel aberrations for numerous recording geometries, wavelengths and recording media. Our experimental results were used to verify the theoretical predictions of computer ray tracing programs. The details of this investigation can be found in quarterly reports 8204-Q-2 and 8204-Q-3. The main results of this effort were summarized in 150 photographs of interference patterns corresponding to various aberration conditions, together with detailed tables giving imaging and aberration data. A number of candidate recording media such as photoresists, dichromated gelatin, and photodegradable polymers were tested by measuring diffraction efficiency and signal-to-noise ratio. Specific

data were reported in quarterly reports 8204-Q-1, 8204-Q-2 and 8204-Q-3. In addition, the optimum preparation and processing of each material was determined. Finally, we constructed and evaluated the imagery properties of a 4X holographic telescope. These results were summarized in a fourth quarterly report, 8204-Q-4.

The investigation of the properties and use of holographic optical elements was extensive. It provided not only quantitative data about the imaging and aberration properties of single holographic optical elements, but also verified the accuracy of theoretical models and demonstrated the practical utility of computer-aided design. We believe that this part of the program provided a solid basis for the future development of holographic optics. Based on the positive results of the first part of the program, we recommended that it be expanded by: (1) Performing a more detailed experimental evaluation of multicomponent holographic elements, (2) Studying fabrication techniques, and (3) Initiating a study of synthetic holographic optical element construction. This report covers the results of the second phase of the overall investigation.

1.1 MULTIELEMENT HOLOGRAPHIC SYSTEMS

Both analytical and experimental data to date indicate that multiple holographic optical elements will be required to perform imaging functions equivalent to those of well-corrected classical optical components. The advantages of holographic optical elements are a savings in weight, space and cost, and the capability for realizing sophisticated and complex design specifications. Procedures for designing multielement holographic optical systems by means of computerized hologram ray tracing techniques are fairly well developed. However, experience

with the fabrication, alignment and testing of multielement holographic optical systems is limited. In addition, many of the optical properties and imaging characteristics of multielement holographic optical systems have not been experimentally verified.

Multielement holographic optical systems are designed in principle to perform a specific function. This function may be, for example, the formation of diffraction-limited imagery of a set of extended, quasi-monochromatic objects. The type, number, spatial position and so forth, of each holographic optical element must be determined by computer-aided ray tracing analyses for any particular application. Suitable computer programs for this purpose have been developed by Latta and Fairchild, and were discussed in quarterly reports 8204-Q-1, 8204-Q-2, and 8204-Q-3. Their algorithms produce designs that minimize the least-mean-square wavefront error for a consistent set of imaging constraints.

Having obtained a realizable multielement design, the overall system must be fabricated. Fabrication consists of a number of steps. First, optical substrates of high quality must be coated with a light-sensitive layer. Then each component of the multielement design must be constructed by exposing the recording medium to a suitable laser interference pattern. In general, each element requires a precise recording geometry. After processing, each element then receives some type of overcoating, e.g., a reflective coating of aluminum with a protective overcoating of silicon monoxide.

When fabrication is completed, the difficult task of alignment must be performed. Experience indicates that careful alignment is required

if the overall imaging performance predicted by the design specifications is to be realized. The most sensitive techniques for achieving this objective are interferometric. The best known example is the Twyman-Green interferometer used for testing conventional lens and mirrors.

Finally, when each element is properly positioned, the multi-element imaging device requires testing. This is accomplished by using one or more st rd procedures such as the Hartmann mask, star, Foucault, Schlieren, and resolution tests. Each test provides different information. For example, the Hartmann test can be used to obtain a quantitative measure of chromatic, spherical and chromatic aberrations. Obviously, these techniques, used for testing conventional optics, require some modification for testing holographic optical elements.

In the present program we have concentrated on the design and construction of a wide-angle, Fourier-transform holographic optical system for use in a Bragg-effect optical memory. The design function was performed by the Environmental Research Ins tute of Michigan (ERIM) according to specifications provided by the Electro-Optics Operation of Radiation. The performance characteristics and geometry of the holographic optical system are discussed in Section II. The construction of the holographic optical system which includes materials, substrate and overcoating considerations and recording techniques is desc.ibed in Section III. Alignment, testing and experimental data are also contained in Section III.

1.2 SYNTHETIC HOLOGRAPHIC OPTICAL ELEME TS

The combination of a computer and precision laser scanner provide an alternative to interferometric methods for constructing

complex holographic optical elements. The basic principles are the following. A holographic optical element is the realization of some prescribed phase variation that can be impressed upon an incident beam of light. For example, a cylinder lens is just the function $\exp(jkx^2/2F)$, where F is the focal length of the lens. The phase variation can be continuous, as in the example just cited, or it can be realized by a finite number of sample values. For a given phase function the computer is used to compute the proper sample values. The output of the computer is used to control a precision laser scanner that writes the desired phase distribution on, for example, a photoresist material. This is a general and extremely powerful technique for realizing complex phase functions for direct imaging or for subsequent interferometric recording. Our exploratory investigation of computer-generated holographic optics is discussed in Section IV.

1.3 CONCLUSIONS

The present program, although scientifically fruitful and certainly comprehensive, must be considered only an initial penetration into a promising area of technology. We believe that holographic optics have the potential to play an important role in a wide variety of scientific endeavors. Specific examples of elementary applications are gratings and large aperture collimators. Two areas that can be exploited immediately and which we recommend for further research are: (1) special purpose, high efficiency blazed holographic grating overcoated for use at vacuum ultraviolet and infrared wavelengths, and (2) synthetic (computer-generated) holograms. Multielement holographic optics is also a promising area; however, we feel that further progress in this area will require a dedicated effort of at least three years at an estimated cost of $500,000. The areas we have recommended for further study

require far more modest support, and could produce valuable unconventional scientific devices in the near term.

The scope of a continuing research effort in the area of holographic optics should center on tasks directed towards both the experimental development of optical devices and instruments and the further development of theoretical concepts. Specific tasks in a statement of work might include the following:

1) Perform an indepth fabrication techniques study with emphasis on substrate materials and the optimization of aluminum and dielectric overcoating.

2) Develop and write general computer programs for recording synthetic holographic optics with a laser scanner. Investigate possible modifications to the Radiation HRMR System to provide a basis for generating synthetic holographic optics for optical computer memory applications.

3) Design, fabricate and test high-efficiency, well-corrected holographic optics of the following type:
   - holographic mirrors, lenses, prisms, beam splitters and lenslet arrays suitable for optical memory applications;
   - blazed, dielectric overcoated gratings for use in the vacuum UV and IR spectral regions; and
   - a large aperture, reflective holographic objective or collimator suitable for use in a specified spectral region.

4) Design, fabricate and test a number of synthetic HOE for specific applications such as a digital phase randomizer or a Schmidt corrector plate for a HOE reflective objective.

SECTION II
HOE DESIGN

2.0 INTRODUCTION

A primary objective of the program was to design and fabricate a holographic optical element (HOE) system suitable for application in an optical computer memory. In particular, we wanted to determine the feasibility of replacing conventional Fourier-transform optics with a holographic analog. The basic specifications for such a system are a low diffraction-limited f/number and a wide field of view. Since the scope of the program precluded the design and analysis necessary to completely achieve this objective, we decided to test the concept with a prototype design. This was accomplished with the aid of the computer-based design and optimization programs developed by Dr. John Latta. The result is a two element, wide-angle reflective HOE system whose specifications and characteristics are discussed in subsequent sections.

2.1 SYSTEM SPECIFICATIONS

This section describes a design for a two element holographic lens system employing reflective hologram elements. The lens system is designed to image an object field at infinity onto a 4 inch film plane at f/20. Although a wide angle lens was requested, implying a half-field of 30^{o} or better, the decision to use reflective elements in a two lens system limited the half-field angle to a maximum of 15^{o}. This is shown by Figures 1a, b, and c which show the lens configuration and light rays for field angles of $\alpha_c = 0$, 10^{o}, and -15^{o}. Field curvature and image aberrations become excessive for field angles $\alpha_c > +10^{o}$; the lens can accommodate, however,

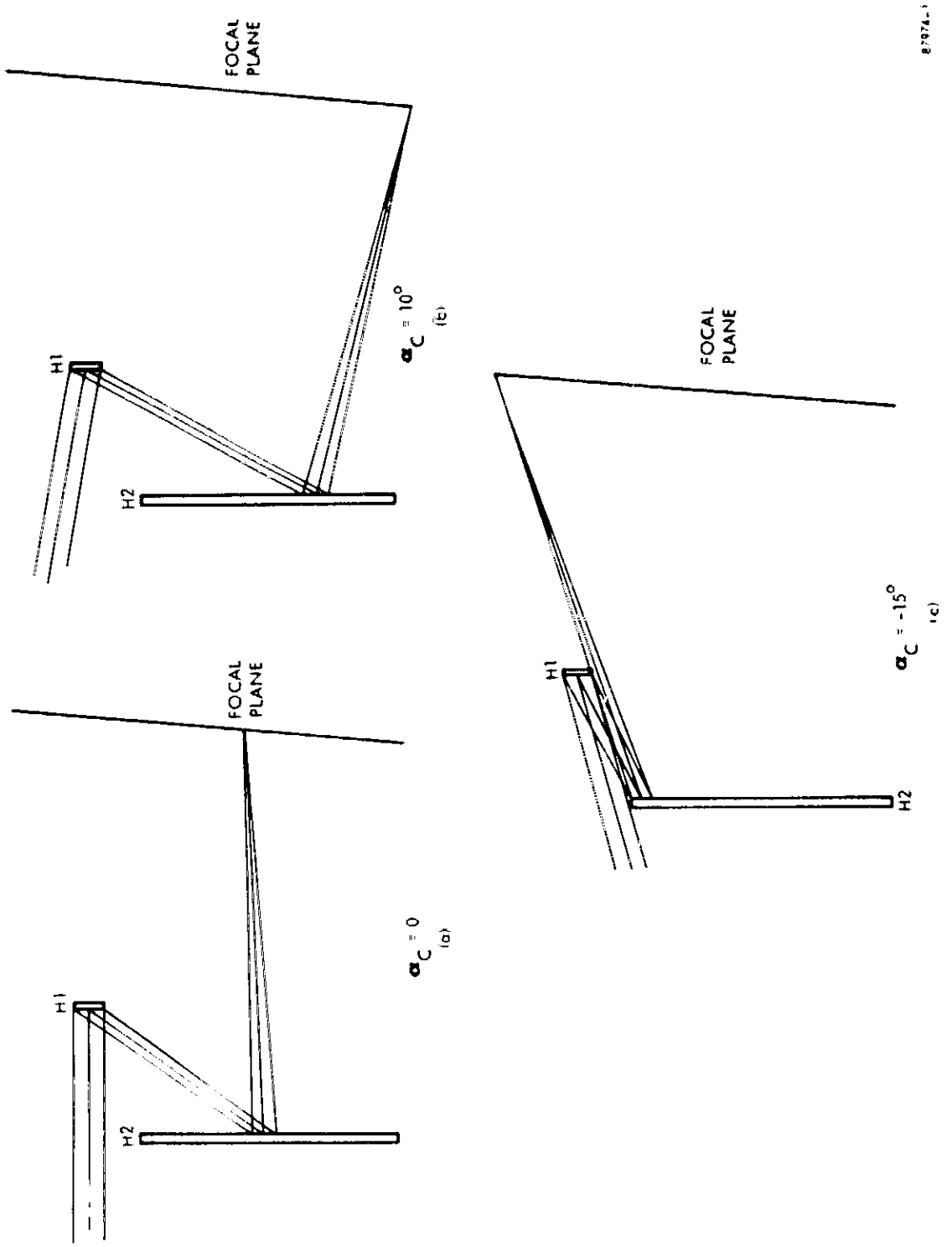

FIGURE 1. GEOMETRY AND MODE OF OPERATION OF A WIDE ANGLE HOLOGRAPHIC OPTICAL SYSTEM.

angles of $-15^{\circ} \leq \beta_c \leq +15^{\circ}$. The system geometry and construction is summarized in Table I.

2.2 SYSTEM PERFORMANCE

Figures 2a and b show the image location Z_i as a function of field angles α_c and β_c, respectively. In the β direction, there is a considerable amount of field curvature symmetrically arranged about $\beta_c = 0$. For sharp focus across the entire field with a flat film, the depth of focus would have to be ± 5 mm, about an order of magnitude greater than can be expected for an f/20 system. In the α direction, there is less field curvature for $\alpha_c < 7.5^{\circ}$, but the image plane is tilted about 5°. This is due to the change in system focal length caused by changes in the distance rays travel between holograms for different field angles α_c. Although this problem exists for conventional optical systems, it is aggravated by the dispersive nature of the holographic optical elements. In addition to field curvature, this lens design also suffers from barrel distortion.

Still more distortion is introduced by the nonlinear variation in creep on H2 with changes in α_c. This has the effect of causing the image plane to be larger in the x-dimension than in the y-dimension for the same range of α_c and β_c. In this design, such distortion is considerable, causing the image plane to be elongated in a 3:2 ratio.

Figures 3a and b show the total wavefront aberrations as a function of α_c and β_c, respectively. With the exception of an anomaly at $\alpha_c = -7.5^{\circ}$, the aberrations are less than 15λ for $\alpha_c \leq 8^{\circ}$, and are less than 8λ for the entire range of β_c. Astigmatism and coma are the dominant terms.

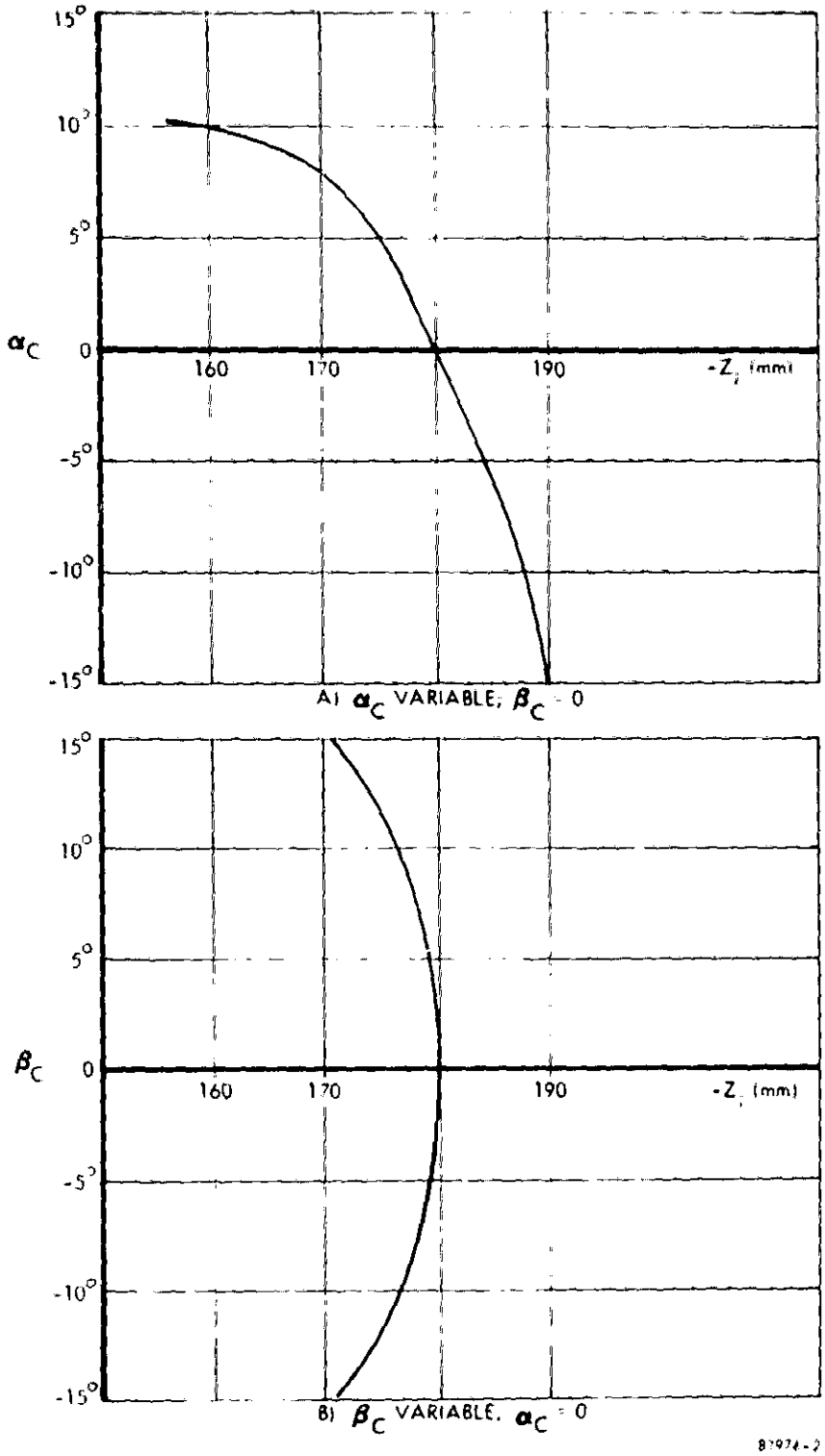

FIGURE 2. FOCAL POSITION AS A FUNCTION OF FIELD ANGLE FOR A WIDE ANGLE HOLOGRAPHIC OPTICAL SYSTEM.

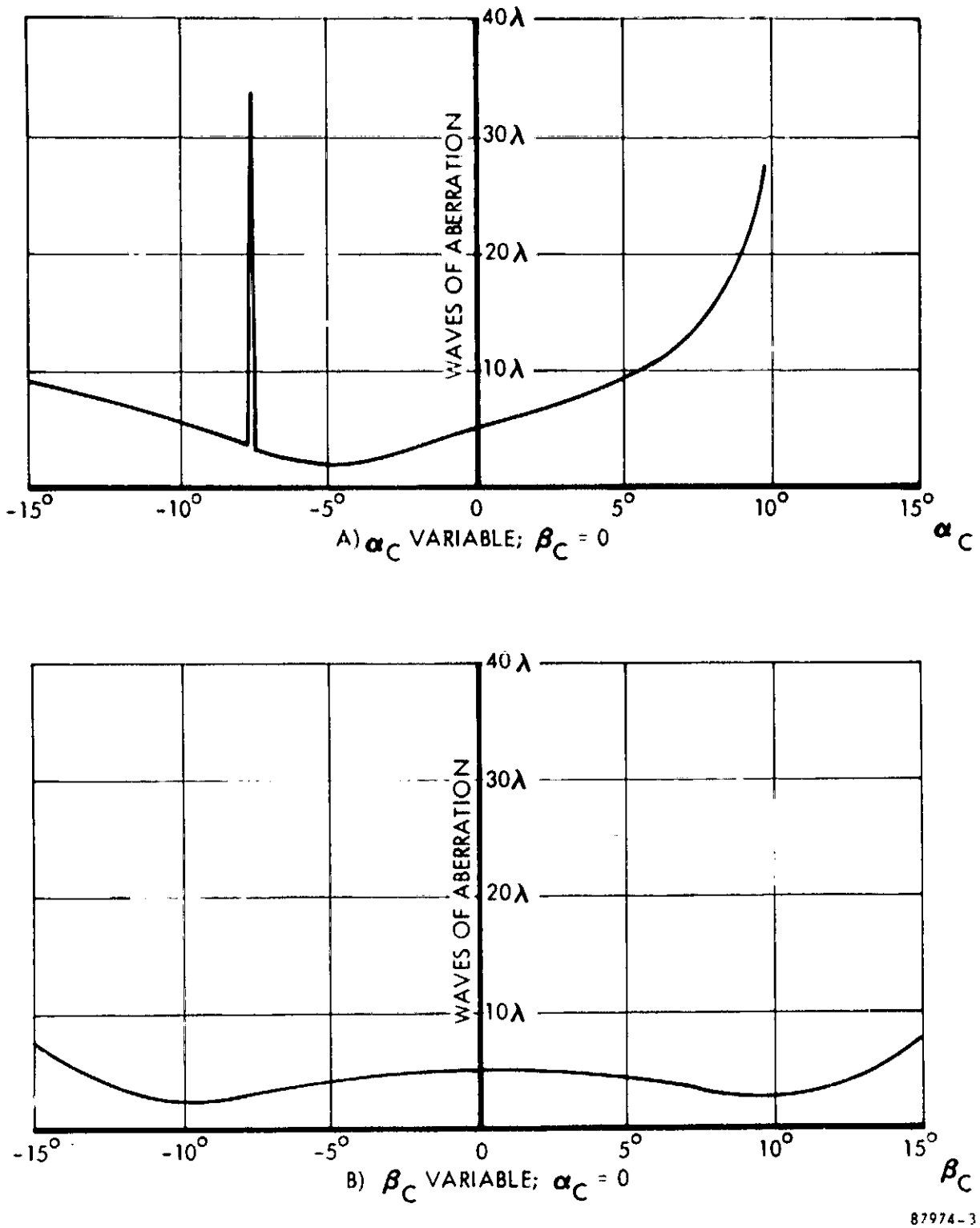

FIGURE 3. TOTAL WAVES OF ABERRATION AS A FUNCTION OF FIELD ANGLE FOR A WIDE ANGLE HOLOGRAPHIC OPTICAL SYSTEM.

TABLE I

HOE PARAMETERS*

HOL 1: $\alpha_o = -45^o$, $R_o = 0.387\,m$

$\alpha_r = 0$, $R_r = +\infty$

DIA = .014 m

ORDER = -1

$\lambda_o = .4579\,\mu m$

HOL 2: $\alpha_o = 0$, $R_o = 0.181\,m$

$\alpha_r = -45^o$, $R_r = 0.290\,m$

DIA = .115 m

ORDER = -1

$\lambda_o = .4579\,\mu m$

SYSTEM: $\alpha_{12} = -55^o$, $R_{12} = .097\,m$

$\lambda_c = .4579\,\mu m$

$R_c = +\infty$

* Construction parameters are α_o , R_o for the signal beam and α_r , R_r for the reference beam. The parameter α_{12} is the angle between the optic axes of the HOE.

A multielement holographic lens system intended to work over a relatively large field of view must be carefully designed so that unwanted diffracted or undiffracted orders do not reach the image plane. High offset angles, volume holograms, and suitably located stops can be used to minimize the problem, but may reduce the lens performance in other respects. Although an offset angle of 45° was chosen for the elements of the lens described here, it can be seen in Figure 1c that the reflected zero order from H2 will strike the film.

Other geometric configurations considered were limited by aberrations of several hundred wavelengths. These configurations included rotation of H2 by 45° or 90° with respect to H1, and specification of equal but opposite bending factors for the holograms. Only the parallel configuration with dimensions close to those of the final system had low aberrations. In fact, an evaluation of Champagne's equations for this system showed astigmatism coefficients that were very nearly equal but opposite for the two holograms, indicating that the relatively low aberrations are due to compensation by the two holograms in the parallel configuration.

The dimensions were chosen so that the image would fit approximately onto 4 inch film. The actual image size in the ζ direction for a 30° field of view is 0.171 m, or 6.93 inches. The dimensions can all be reduced by a scale factor to cover smaller film sizes.

2.3 CONCLUSIONS AND RECOMMENDATIONS

This study can only be considered as a preliminary approach to the problem of designing a wide angle lens using holographic lens elements. Although the aberrations are probably tolerable for many

applications, the field curvature and distortion are probably too great for most applications. It may be possible to reduce the aberrations still further by slight modification of the geometric parameters to provide even better aberration compensation by the two elements. Image distortion may be reduced by locating a stop between the lens elements, and by altering the relative positions of the two elements. It may be possible to reduce the field curvature by increasing the symmetry of the bending factors of the elements, although this may greatly increase the lens aberrations.

The 30° field of view is not very large for a wide angle lens. It nevertheless seems unlikely that the field of view can be increased significantly in the α-direction for a system employing two thin hologram elements operating in the reflective mode. A true wide angle design employing a multielement holographic lens system may not be possible even in transmission, however, because of the problem of preventing unwanted orders from reaching the image plane for all field angles.

We believe that further study of the wide angle lens problem should be carried out in the following steps:

1. Determine whether a geometrical configuration can be developed that prevents unwanted diffracted orders from reaching the image plane.
2. By use of a suitable configuration of hologram parameters and stops consistent with step (1), reduce the field curvature and distortion of the lens system at a minimum cost in aberrations.
3. Investigate the effects of a wavelength shift on the lens performance.

SECTION III
HOE EXPERIMENTS

3.0 INTRODUCTION

In this chapter we summarize the experimental work required for the fabrication and testing of the multicomponent reflective HOE system. First, hologram recording materials are discussed. Then we describe the basic elements of HOE fabrication which include substrate selection, hologram recording and aluminum overcoating. Finally, experimental activities related to the alignment and the measurement of imaging properties of the HOE system are discussed and experimental data presented.

3.1 RECORDING MATERIALS

The performance of holographic optical elements depends greatly upon the characteristics of the recording material. Our initial plan was to construct holograms only in photoresist; however, we decided that the high levels of diffraction efficiency and signal/scatter noise ratio of HOE fabricated from dichromated gelatin were too attractive to ignore. Although we later discovered problem areas that restrict the general use of this material, we include our findings for completeness sake.

3.1.1 Dichromated Gelatin

Dichromated gelatin is one of the best available volume phase recording materials, and is characterized by both high diffraction efficiency with negligible insertion loss and high maximum signal-to-noise ratio. It can be used to record zone plates with a carrier frequency in

excess of 6000 ℓ/mm (Lippmann-Bragg holograms). Holograms recorded in dichromated gelatin possess reconstruction parameters comparable to the best volume phase media such as photodegradable plastics.

Dichromated gelatin layers are prepared by a number of methods. Of the many possible methods, the one due to Chang[1], which is summarized in Table 2, has yielded the most consistent and highest quality results. Chang's method of preparation begins with a Kodak 649F plate. The silver halide is removed by fixation, leaving the gelatin matrix. The gelatin is hardened and then dichromated.

Hardened gelatin films sensitized with ammonium dichromate are used to record holograms by simply exposing the prepared plates to a predetermined average exposure level. The spectral response of the gelatin film allows exposure with light within the 350 nm to 550 nm wavelength region. Low efficiency holograms are produced immediately upon exposure due to crosslinkage of the gelatin molecules. Subsequent chemical processing, such as that reported by Lin[2], and listed in Table 3, greatly enhances diffraction efficiency. The chemical processing of holograms recorded in dichromated gelatin causes a layer splitting or cracking to occur in the gelatin. This phenomenon is unique to dichromated gelatin, and is responsible for the high diffraction efficiencies obtained.

Initial attempts were made to fabricate the wide-angle holographic lens system using dichromated gelatin as the recording medium. This effort was motivated by the hope of simultaneously obtaining good lens performance and high diffraction efficiency comparable to that of a conventional optical element. The construction parameters of the holographic lenses were altered to allow recording the holograms with

TABLE 2

SUMMARY OF CHANG'S METHOD FOR THE PREPARATION OF DICHROMATED GELATIN LAYERS

1. Fix in Part A of Kodak Rapid Fixer a Kodak 649F photographic emulsion for 10 minutes.
2. Wash with running water at 90°F for 15 minutes. Start at 70°F and raise temperature at approximately 2.5°F/min. to 90°F.
3. Stand in air 1 minute.
4. Rinse in distilled water with 2 drops per liter of Kodak Photo-Flo 600 for 30 seconds.
5. Dry completely in room environment.
6. Soak in room temperature water for 2 minutes.
7. Harden in both Part A and Part B of Kodak Rapid Fixer for 10 minutes.
8. Wash for 15 minutes at 70°F in running water.
9. Rinse in Kodak Photo-Flo solution for 30 seconds.
10. Dry overnight at room temperature.
11. Soak plates for 5 minutes in 5% ammonium dichromate solution with 2 drops per liter of Kodak Photo-Flo 600.
12. Wipe ammonium dichromate off glass side of plates.
13. Dry at room temperature for at least 4 hours.

TABLE 3

LIN'S DEVELOPMENT PROCESS FOR HOLOGRAMS
RECORDED IN DICHROMATED GELATIN

1. Rinse in a 0.5% solution of ammonium dichromate for 5 minutes.
2. Bathe with agitation in Kodak Rapid Fixer for 5 minutes.
3. Rinse in water for 10 minutes.
4. Dehydrate in a 50/50 solution of water and isopropanol for 3 minutes.
5. Dehydrate in 100% isopropanol for 3 minutes.
6. Free air dry for 1 hour.

the 488 nm line of an argon laser in a reflective type geometry. Direct recording of the elements in a reflective mode would eliminate the overcoating process required by photoresist holograms. To avoid the need for high quality, low f/number lenses to provide converging beams for recording, the design was further altered to allow formation of the hologram using the conjugate wave forms of the desired diffracted waves. This allowed construction using diverging spherical waves, and read out using the conjugate wave. An additional advantage of recording holograms in a reflective mode is that the Bragg angular sensitivity could be minimized using a larger exposure than that necessary to obtain 100% diffraction efficiency. As Kogelnik[3] has shown, this is accounted for by the broadening of the angular sensitivity as the index of refraction modulation is increased.

Holographic optical elements were recorded in dichromated gelatin in volume reflection hologram geometry. To eliminate the effect that high levels of humidity have on the hygroscopic gelatin, the holograms were sealed with optical cement and a clean cover glass. This was done after chemical processing and complete drying of the hologram. The processed hologram was placed in the recording geometry, and when the Bragg condition was satisfied for the recording conditions the hologram was sealed. Although the diffraction efficiencies for holograms prepared in this way were consistently near 90%, aberrations of the diffracted waveform were severe.

The causes of the observed aberrations are unknown, although some probable reasons can be stated. For example, since the holographic element was illuminated by the conjugate wave form, any phase change of the incident wave caused by passage through the glass substrate would result in aberrations of the diffracted wave. Also, curing of the optical

cement used to seal the hologram may have had an effect on the micro-fringes recorded in the hologram. This would have caused the fringes to distort which, in turn, would produce aberrations in the diffracted wave. The existence of uncompensatable aberrations in the holographic elements recorded using this method indicates fundamental limitations with respect to optical quality. A partial solution is the use of well polished optical plates as substrates.

3.1.2 Shipley AZ1350 Photoresist

Shipley AZ1350 photoresist has the major advantage of dimensional stability when compared with gelatin. All gelatin materials absorb water during processing which causes them to swell, and changes the apparent grating frequency. Photoresist is developed by etching away material in the exposed regions forming a relief grating of exactly the frequency recorded. The Shipley photoresist was selected for final hologram construction.

Photoresist is a planar phase recording material; this limits diffraction efficiency to 34% in each beam. A planar hologram recorded in a photoresist diffracts backward as well as forward waves, and the back diffracted beam can be enhanced by a reflective overcoating.

The existence of back diffracted beams allows a transmission hologram to be recorded, rather than a reflection hologram to construct the HOE system. The transmission hologram is recorded with a 45° offset giving a spatial frequency of 1650 ℓ/mm; a reflection hologram would be recorded with a 135° offset (spatial frequency of 4000 ℓ/mm). The lower spatial frequency reduced the recording stability requirements which were important due to the long exposure times required.

AZ1350 is primarily a UV sensitive media, and was therefore used at 457.9 nm. This is the wavelength for which the HOE system was designed, but is a low power line of the argon laser. Therefore, exposure times of 30 minutes and 90 minutes were needed for recording the small and large elements, respectively.

Past experience has shown that 1 μm thick resist layers are optimum for holographic recording. Thinner coatings reduce efficiency, while thicker coatings, in general, have poor surfaces. One micron layers can be obtained in three ways: spinning, dipping, and gravity flow coating.

Spinning, commonly used in the micro-electronics industry, has two major disadvantages for holographic purposes. First, it cannot be used to coat large substrates because they have too much inertia to be accelerated rapidly enough for uniform coatings. Second, centrifugal force aligns solid particles on radial contours. The radial alignment generates a circular noise pattern.

In dipping, the substrate is lowered into a solution and drawn out at a constant speed. The thickness is controlled by the drawing rate, faster rates yielding thicker coatings and conversely. For one micron layers, the substrates were pulled at 34 cm/minute. Dip coating provides layers which are uniform across the plate, but thicker at the bottom due to gravity. Figure 4 shows a typical wedge pattern for a 75 x 100 mm^2 plate, as measured with a Leitz reflecting interference microscope.

For a higher level of uniformity over the center of a substrate, flow coating is best. This requires carefully leveling a glass substrate on a flat surface, and setting the boundaries with a metal dam forming a 45° angle with the surface to be coated. The resist is poured into the center of this dam and the plate is tightly covered and allowed to dry in

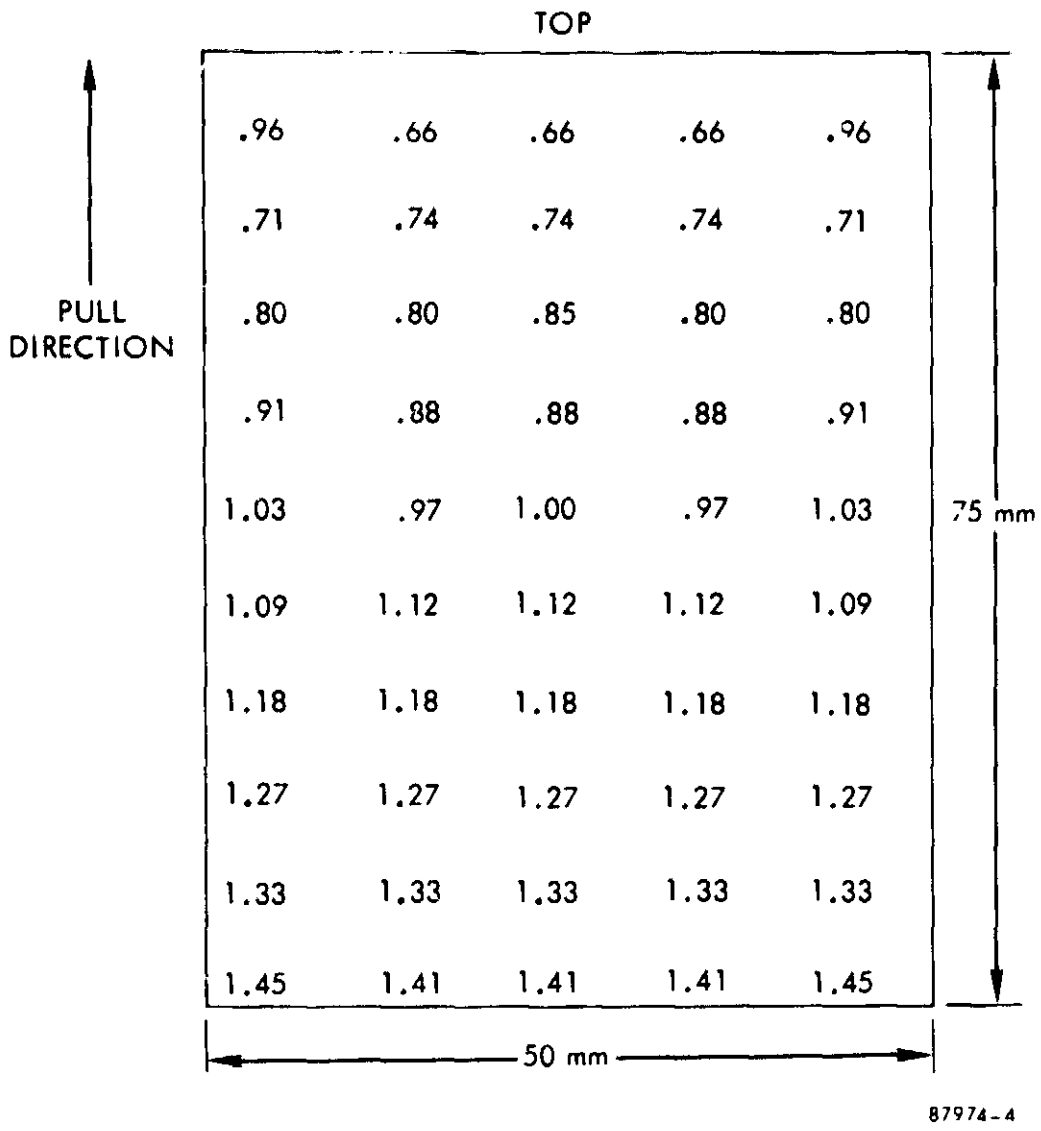

FIGURE 4. THICKNESS PROFILE FOR SHIPLEY AZ1350 DIP COATED ON A 50 mm x 75 mm GLASS SUBSTRATE (RELIEF IN μm).

a strong solvent atmosphere. Gravity causes the liquid to spread uniformly over the plate with a thicker wave at the edges. The coating uniformity obtainable with flow cast layer is shown in Figure 5.

Flow casting is the only reasonable way to coat very large substrates, but it presents problems. The plates must be allowed to dry very slowly (3 hours compared to 3 minutes for dip coating) to prevent the formation of orange peel. However, Shipley photoresist when liquid carries a static charge which attracts dust. It requires extreme clean room conditions to cast a dust free coating. For these reasons we chose to dip coat our plates.

Whichever method is used, the substrates must be rigorously cleaned prior to coating. The procedure we used is as follows:

1. Soak for 1 hour in a hot enzyme active alkaline solution.
2. Soak for 1 hour in aqua regia to neutralize the surface.
3. Rinse in distilled water.
4. Rinse in acetone.
5. Rinse in two successive baths of methanol.
6. Blow dry with filtered nitrogen.
7. Bake 30 minutes at 100°C to remove any trace of water.
8. Dip coat – free air dry 3 minutes.
9. Bake 10 minutes at 125°C to harden.

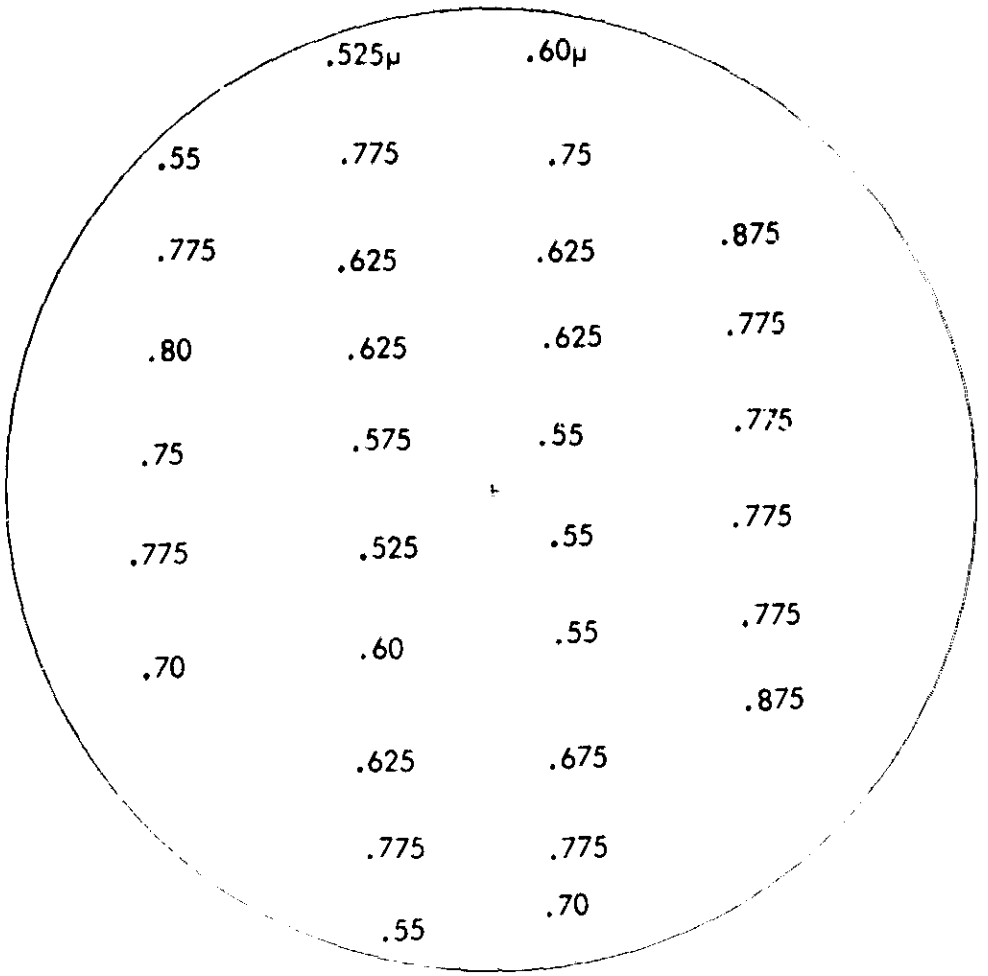

FIGURE 5. THICKNESS PROFILE FOR SHIPLEY AZ1350 FLOW COATED ON A 100 mm DIAMETER GLASS SUBSTRATE (RELIEF IN μ m).

3.2 SUBSTRATES

Kodak precision photographic glass plates were used as substrates since they provide sufficient dimensional stability and flatness. Glass is extremely rigid at ordinary temperatures with a humidity coefficient that is effectively zero and thermal coefficient of expansion of only 4.5×10^{-6} cm per cm per degree Celsius. Gelatin was stripped off using a mild sodium hydroxide solution to prevent pitting, and the plates were cleaned and coated as specified in Section 3.1.2.

The first element was recorded on 50 mm x 50 mm x 1.5 mm precision flat plates. Tests showed these plates to be flat to much less than 1λ per centimeter. This slight nonuniformity is constant throughout recording and reconstruction, and is not objectionable. A more serious problem is the possibility of warping. When these glass substrates are subjected to stress such as that characteristic of a hologram plateholder, warpage results. When this occurs, the reconstructing surface will be slightly different from the recording surface causing aberrations. The second element was recorded on 10 cm x 12.5 cm x 0.625 cm microflat plates. These plates are specified flat to 0.4λ per centimeter. Since they are thicker, warping should be less of a problem.

3.3 HOLOGRAM CONSTRUCTION

The holographic lens system discussed in Section II was constructed in two parts. In order to simplify realignment, we recorded the second element first. In this way, the first element could be read out within the original geometry used to record it; this reduced residual aberration to a minimum value.

The recording setup for the second element is shown in Figure 6. A Coherent Radiation Model 52 argon ion laser was used as a coherent light source. An electro-mechanical shutter with a 1 ms to 10 s range was used for turning the laser beam on and off, a convenience utilized both for hologram recording and the photographic exposure of interference patterns. A small portion of the laser beam was used for monitoring laser power and mode structure. The remainder of the laser beam was divided into a reference and a signal beam to form matched interferometer paths. Each path provided a spatially filtered spherical wave with a 100 mm diameter at the recording plane. The objectives forming the point sources were mounted on micropositioners supported by a rail and platform; this allowed accurate positioning of the point sources. The first source was at 18.1 cm at an angle of 90°. The second source was located 29 cm away from the hologram and had an average angle of incidence of 45°.

The hologram plateholder is designed to provide translational and rotational motion. It accepts 10 cm x 12.5 cm substrates, has X-Y adjustment and is mounted on a Troyke rotary table. This system permits accurate centering of the hologram and alignment normal to the signal beam. The latter was important because this element would require subsequent realignment.

The recording geometry for the lead element is shown in Figure 7. The point source at 45° was moved back to 38.7 cm while the normally incident beam was collimated. Since this setup would be used for reconstruction as well as recording, the plateholder had to allow accurate repositioning after processing. It was therefore designed to provide both translational and rotational degrees of freedom. The

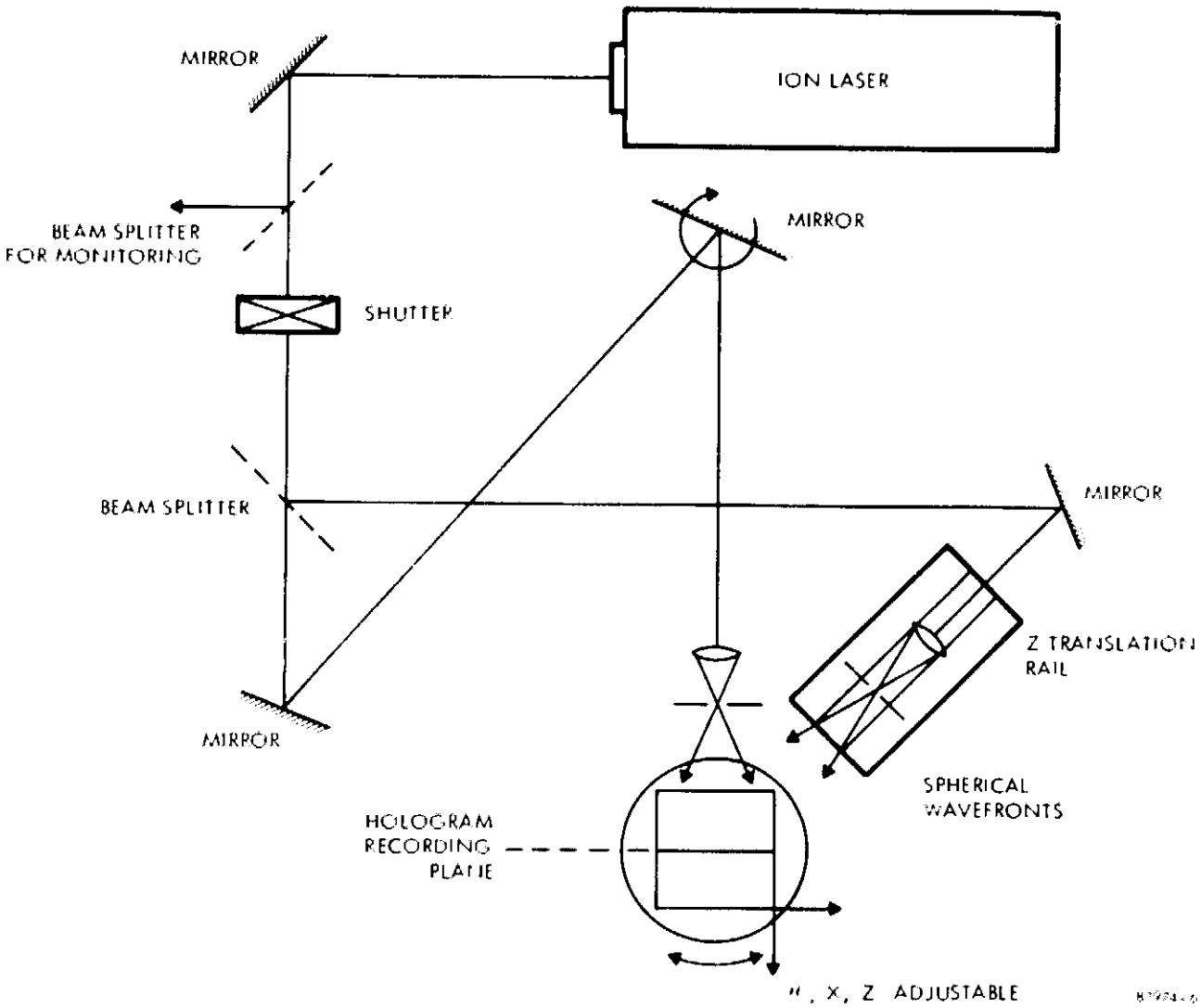

FIGURE 6. EXPERIMENTAL SETUP USED TO RECORD THE SECOND ELEMENT OF THE HOE SYSTEM.

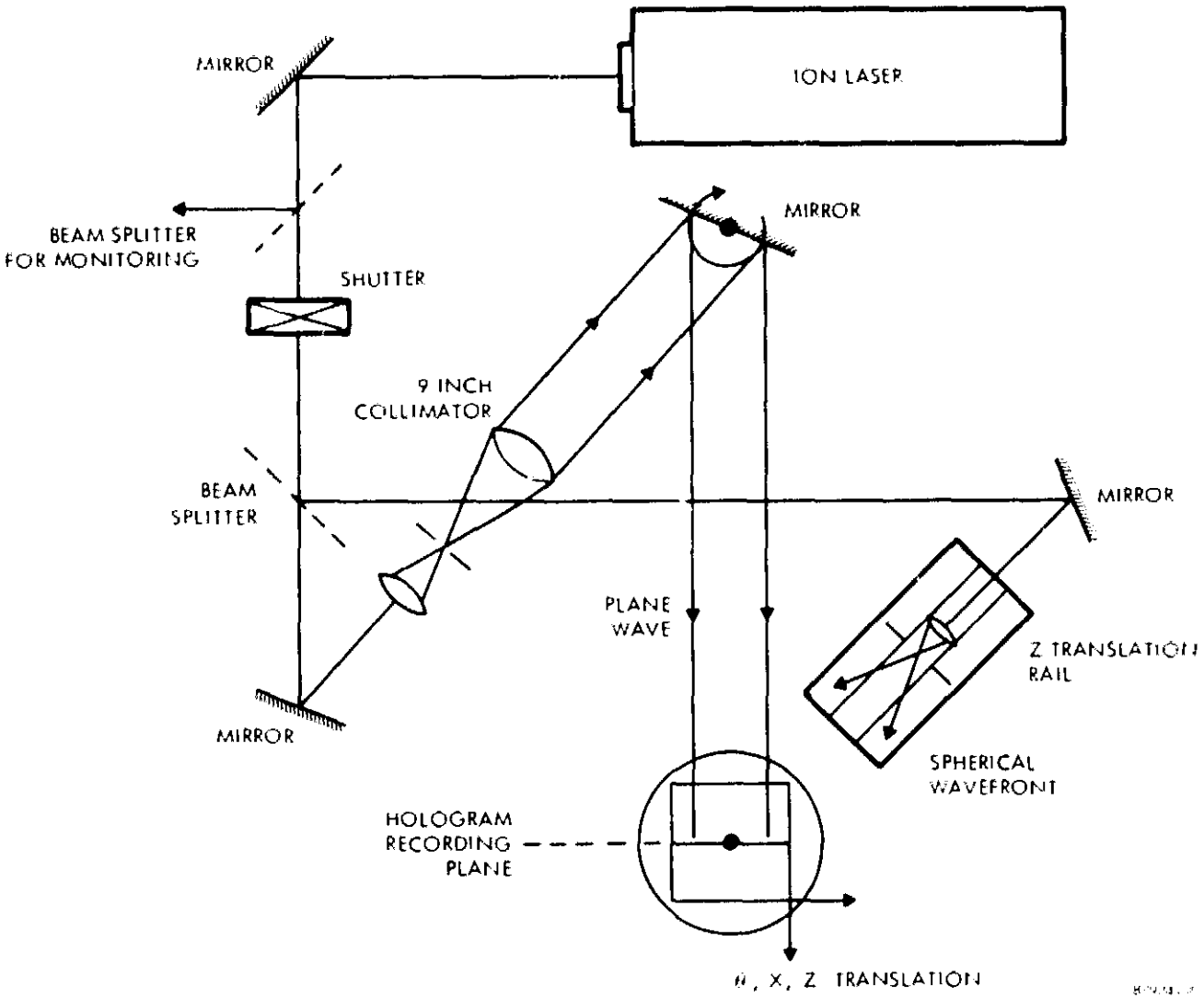

FIGURE 7. EXPERIMENTAL SETUP USED TO RECORD THE FIRST ELEMENT OF THE HOE SYSTEM.

plateholder accepts 50 mm x 50 mm plates with a clear aperture of 45 mm diameter. We attached the plateholder to a Lansing gimbaled mount that in turn was placed on top of X-Z Lansing translation stages. The entire assembly was mounted on a Troyke rotary table. A platform and rail were available for course X-translation.

The recording material was held in the plateholder by means of three thumb screws. Repeatability of position was obtained by resting the recording material substrate on three pins. This permitted the removal of the exposed recording material for chemical processing and subsequent replacement with good precision.

At 457.9 nm, AZ1350 requires 200 mJ/cm^2 exposure for optimum reconstruction parameters. Thus, the first element of the HOE system required a 30 minute exposure, while the second element required a 90 minute exposure. We were able to reduce exposure by a factor of two using UV pre-exposure. The plates were exposed for one second to a B100 Spectroline mercury vapor lamp. The uniform pre-exposure, when added to the holographic exposure, gave a total exposure of 200 mJ/cm^2. This technique has the disadvantage of increasing the effective K-ratio of the two beams from 1 to approximately 6 .

After exposure, the plates were processed using undiluted 1350 developer. Trial and error experimentation showed the optimum development time to be 60 seconds. The plates were then thoroughly rinsed with distilled water and free air dried. They were then overcoated.

3.4 ALUMINUM OVERCOATING

Since the interference pattern is etched into photoresist, it is possible to overcoat it with aluminum to enhance the efficiency of the

back diffracted beams. The diffraction efficiency of the second element of the HOE system was measured before and after overcoating in an experiment to determine the degree of improvement. An interesting result is the following:

Order of Back Diffracted Beam	Efficiency Before Coating	Efficiency After Coating
+1	0.7%	13%
-1	0.7%	7.3%

There are two techniques available for overcoating photoresist holograms with aluminum: sputtering and evaporation.

Sputtering is accomplished by bombarding a target with energetic particles (positive argon ions) causing surface atoms to be ejected. These atoms deposit on any surface close to the target. The aluminum target is larger than the resist plate, so the resulting film is extremely uniform. Since the target can be any reasonable thickness, films of up to 3 μm can easily be deposited. Sputtered films have higher quality than evaporated films since they are more uniform and adhere better; however, the entire coating chamber is heated to approximately 200°C which could damage the resist. Therefore, we chose to coat the plates by evaporation.

Evaporated films are the result of heating the aluminum in a vacuum chamber until a large number of atoms leave the aluminum surface, and are deposited on a substrate suspended above. Since only a small amount of aluminum can be heated, it acts more like a point source. The resulting layers are limited to 1 μm and are somewhat less uniform than

sputtered films. However, the heat is localized at the vapor source which makes this technique safer for coating photoresist materials.

Aluminum does not adhere well to photoresists. We therefore found it desirable to lay down a thin layer of chrome first. This is a common practice to increase adhesion, and does not affect the efficiency of a front surface element. For our lenses, a 10 nm chrome film followed by a 100 nm aluminum film was evaporated onto the photoresist hologram.

As soon as the aluminum is exposed to air, a thin oxide layer is formed on the surface. This hard layer does not affect the quality of the coating, but does protect it from further chemical damage. However, the oxide layer remains susceptible to mechanical damage. If the overcoated holograms require frequent handling or cleaning, they must be overcoated with silicon monoxide to prevent damage.

Both the quality and adhesion of the overcoatings depend critically upon the cleanliness of the surface to be coated. Since it is impossible to subject photoresist to stringent cleaning procedures, care must be taken to minimize handling prior to overcoating. In practice, we found the cleaning procedures for the glass substrate to be of primary importance. If the glass is cleaned with a solvent saturated cloth, transparent streaks of solvent may dry on the surface. This film does not become apparent until the plate is overcoated with aluminum, then it gives the appearance of deep scratches on the surface. The cleaning procedures that worked best were outlined in Section 3.1.2.

3.5 ALIGNMENT PROCEDURE

After the multielement holographic lens system was recorded and overcoated as previously described, the individual holograms must be

replaced in the recording geometry and aligned. The alignment of the elements must be accomplished precisely if the holographic optical elements are to provide optimum performance. The alignment of the wide angle holographic lens system was performed using the classical methods of the Hartmann test and the modified Twyman-Green interferometer. The Hartmann test allowed positioning on a preliminary basis, while the interferometer provided a means of detecting misalignments that cause small phase errors. This section details the experimental methods used to align the multielement holographic lens system and the results obtained.

3.5.1 Interferometric Alignment Test

The method chosen to position the front element of the wide angle lens system was a modified Twyman-Green interferometer. The interferometric technique allowed precise alignment of the front element on the optic axis. The configuration of the optical equipment for performing the interferometric alignment is shown in Figure 8.

After the holographic lens was overcoated the plate was reinserted into the recording geometry in approximately the same position as during the exposure process. The addition of a cube beamsplitter into the reference beam allowed observation of the interference pattern between the specularly reflected reference beam and the signal beam diffracted by the hologram.

There are several advantages to this type of interferometric approach. Pathlength equalization in the interferometer is automatically accomplished. The fundamental waveforms used to form the interference pattern are similar. Also, the fringes are localized in the plane of the holographic optical element.

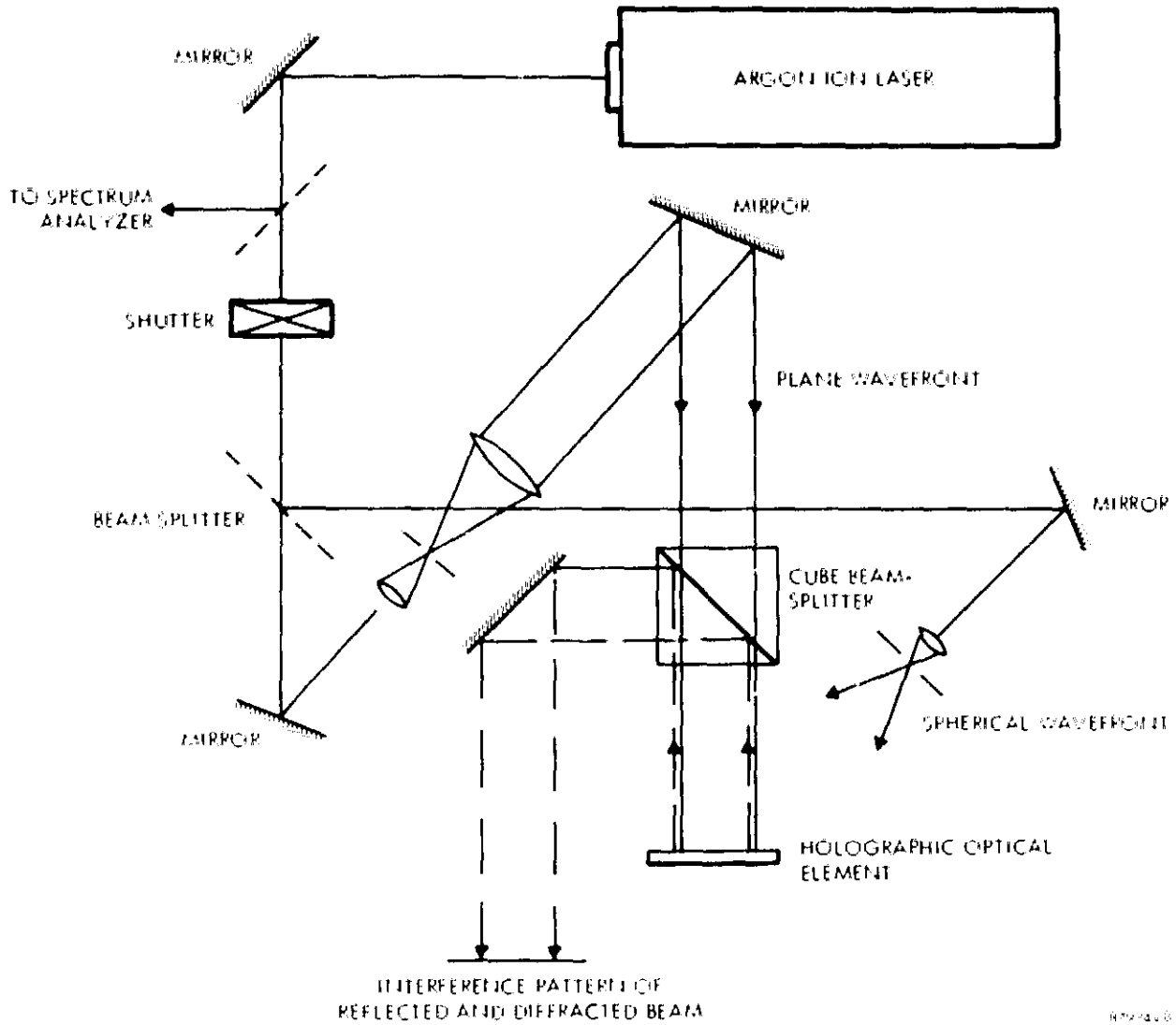

FIGURE 8. ARRANGEMENT OF OPTICAL EQUIPMENT USED FOR INTERFEROMETRIC ALIGNMENT.

The plateholder the holographic lens was mounted in allowed precise positioning of the lens on the optic axis. Initial positioning of the processed hologram in approximately the same position and orientation as during recording was insured by three pin registration on the plateholder. The holder was comprised of an X-Y-Z Line Tool micropositioner onto which was mounted a Lansing gimballed mount that held the hologram. The micropositioner provided translational movement accurate to 2.5 μm on each axis; while the Lansing gimballed mount provided two independent rotational adjustments accurate to 0.02 mrad.

An interference pattern was observed between the diffracted and specularly reflected beam when the processed hologram was replaced in the plateholder. Small adjustments of position and orientation of the hologram yielded the bright field condition corresponding to on-axis alignment. A photograph of the bright field interference pattern is shown in Figure 9. The dimension of the interference pattern corresponds to the full diameter of the hologram, and indicates the zero fringe condition over a 2.5 cm aperture of the holographic lens.

The imaging performance of the aligned element was investigated by examining the structure of point images as a function of aperture size, and by testing the resolution of a single holographic lens. A collimated beam of adjustable diameter was incident normally on the holographic lens. The lens diffracted a beam at an angle of 45 degrees which was brought to focus a distance of 39 cm away. A microscope objective then imaged the focused point onto a film plane. Photographs of point images at the focal point are shown in Figures 10 and 11. Figure 10 is a photograph of a point source image with the lens focusing a collimated beam at f/20. The waves of aberration seen in the

FIGURE 9. BRIGHT FIELD INTERFERENCE PATTERN CORRESPONDING TO ON-AXIS ALIGNMENT

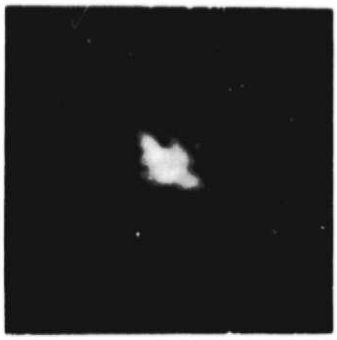

87974-10

FIGURE 10. MAGNIFIED VIEW OF POINT FOCUS PRODUCED BY THE FIRST HOLOGRAPHIC OPTICAL ELEMENT AT f/20

87974-11

FIGURE 11. MAGNIFIED VIEW OF DIFFRACTION LIMITED SPOT PRODUCED BY THE FIRST HOLOGRAPHIC OPTICAL ELEMENT WHEN APERTURED TO f/50

photograph are probably caused by a lack of flatness of the aluminized photoresist/glass surface of the reflective element. Flatness of the glass plates used as a substrate for the photoresist was nominally less than 1 wave per centimeter. The front element produced a diffraction limited point focus as shown in Figure 11 when apertured to f/50. The resolution of the front lens was tested by imaging an USAF 1951 Resolution Test Chart using a Fourier transform geometry. The image was examined visually using a microscope. The lens resolved as high as Group 3, Element 6 corresponding to 14.25 ℓ/mm.

3.5.2 Hartmann Alignment Test

The use of the Hartmann Mask Test, instead of interferometric techniques, to align the second element of the holographic lens system was dictated by the low intensities available at 457.9 nm; the typical throughput diffracted power levels of the lenses were in the 100 nW range. This low intensity made visual observation of an extended interference pattern difficult. The Hartmann test provided a convenient method for positioning the second element given the low power levels available, since observation was made at the point focus, effectively increasing the power level per unit area.

The Hartmann mask test simulates a ray tracing operation. In practice, a specially constructed diaphragm is inserted into a collimated beam incident on an optical element. The diaphragm is an opaque mask in which several holes approximately a millimeter in diameter have been made in selected locations. Thus, only selected rays are allowed past the diaphragm and are incident on the optical element. The positions of these rays after passage through the optical system can be adjusted for an optimum condition by shifting or reorienting the

optical element. Quantitative data about gross aberrations can be obtained by monitoring the positions of the rays relative to the optic axis.

The initial position of the second element was set to conform to the dimensions given in the lens design supplied by ERIM. The second element was mounted in a plateholder that allowed micrometer translations in three directions and two independent rotational adjustments.

For the alignment of the second element in the wide angle lens system the Hartmann mask had five holes, each approximately 1 mm in diameter. One of the holes defined a center, while the other four were equally spaced around a circle corresponding to an f/20 aperture for the system. The geometry used for the alignment is shown in Figure 12. The addition of a mirror (flat to $\lambda/4$) was necessary to fold the optic axis to allow direct microscopic examination of the point focus.

The alignment was performed by examining the point focus of the Hartmann mask. Movement of the microscope along the optic axis showed the sagittal and tangential foci and the circle of least confusion. Ideally, in the back focal plane, all five rays passed by the Hartmann mask would be brought to focus by the lens system to the same diffraction-limited spot. Since the holes in the Hartmann mask were small in diameter, what was observed in the back focal plane were five diffraction limited points. The position of the second element was adjusted in a raster type scan until the image in the back focal plane was as close as possible to the ideal single diffraction limited point. Examination of the Hartmann mask image a meter from the focal point revealed no astigmatism within the experimental accuracies of the test.

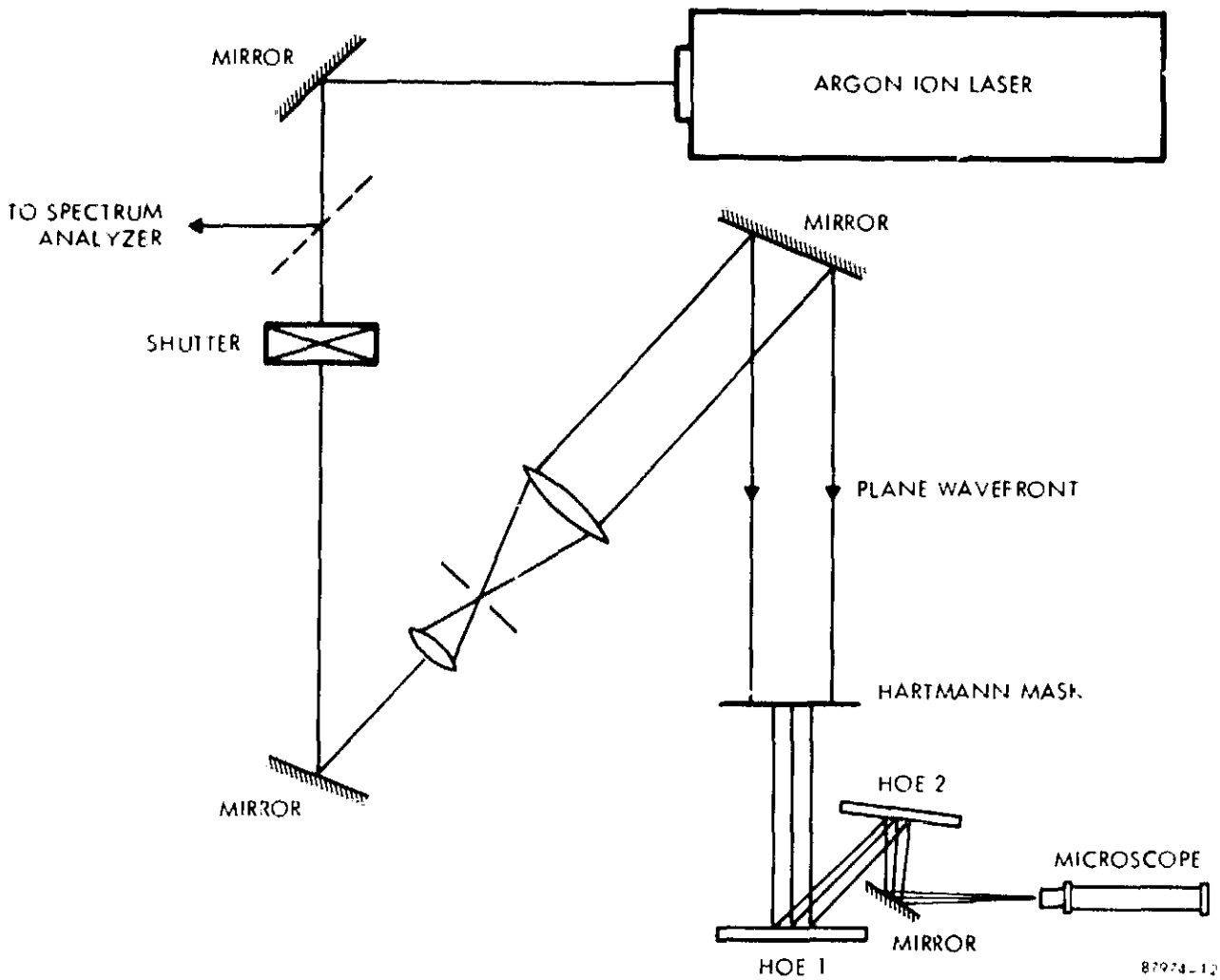

FIGURE 12. EXPERIMENTAL GEOMETRY USED FOR THE HARTMANN ALIGNMENT.

3.6 RESOLUTION MEASUREMENTS

The resolution of the wide angle holographic lens was experimentally measured by using the lenses to image an USAF 1951 resolution test chart in a Fourier transform type geometry. The measurements were performed with a coherent collimated beam of 457.9 nm light that was amplitude modulated by transmission through the resolution chart. The beam was incident on the lens for a variety of field angles. The resolution for each angle was determined by microscopic examination of the refocused image after passage through the lens system. The measurements were made for an aperture of f/20. The data are summarized in Table 4.

From Table 4 we see that the resolution on axis of 16 ℓ/mm decreases to 6 ℓ/mm as the angle of incidence changes by 15 deg in the α_c - direction, the plane perpendicular to both elements. As the angle β_c is changed the resolution is degraded from 16 ℓ/mm for an axis imaging to 9 ℓ/mm for β_c = 10 deg.

A photograph of a section of the target image is shown in Figure 13 for the field angles α_c = -15 deg, β_c = 0 deg. A microscope objective was used to enlarge the aerial image formed of the resolution target by the holographic lens system. The Group 2, Element 5 shown in the photograph is resolved.

3.7 MONOCHROMATIC POINT IMAGING

The monochromatic point imaging properties of the aligned holographic lens system were measured as a function of field angle. A well-collimated coherent beam of 457.9 nm light was used to illuminate

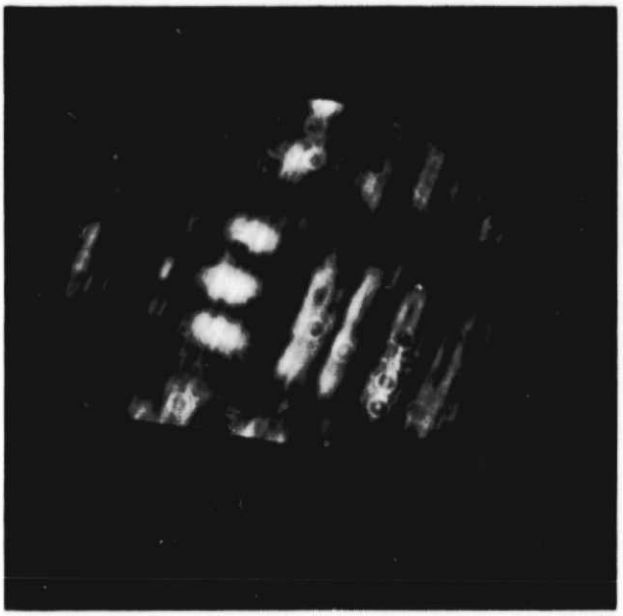

87974-13

FIGURE 13. MAGNIFIED VIEW OF THE IMAGE PRODUCED BY HOLOGRAPHIC OPTICS WHEN THE STANDARD 1951 AIR FORCE RESOLUTION TARGET IS IN THE FRONT FOCAL PLANE OF LENS

TABLE 4

RESOLUTION OF THE f/20 WIDE ANGLE HOLOGRAPHIC LENS SYSTEM VS. THE FIELD ANGLES α_c AND β_c

Field Angles (deg)		Resolution	
		Group Element	ℓ/mm
α_c	β_c		
0	0	4-1	16
+6	0	3-6	14
-6	0	3-4	11
+15	0	2-5	6
-15	0	2-5	6
0	+5	3-4	11
0	+10	3-2	9

(Measurements were made using a USAF 1951 resolution target coherently illuminated with 457.9 nm light. The target was reimaged in a Fourier transform geometry by the holographic lens system.)

the holographic elements at several field angles. An adjustable iris in the incident beam provided the means of studying the point imaging abilities of the lenses as a function of f/number. Microscopic inspection revealed the quality of the point focus. The experimental geometry used for the test was identical to that shown in Figure 12 except the adjustable iris replaced the Hartmann mask.

The point focus of the holographic lens was diffraction limited only for apertures less than the f/20 value specified in the lens design. The lens system f/number for diffraction limited performance as a function of field angle α_c with $\beta_c = 0$ is shown in Figure 14. The lens system provides a flat diffraction limited response at f/50 over an angular field of 12 degrees in the α_c - direction, with the f/number increasing for larger angular fields. The behavior for the β_c - direction is similar and is shown in Figure 15.

For photographs, a microscope objective was used to refocus an enlarged point image on the film plane. A series of photographs of the resulting image is presented in Figures 16 and 17 for various aperture sizes and field angles. In Figure 16(a) the circle of least confusion obtained with f/20 for on-axis imaging is shown. In Figure 16(b) and 16(c) the sagittal and tangential foci, respectively, are shown for on-axis imaging at f/20. The lens system becomes diffraction limited as shown in Figure 16(d) when the aperture is decreased to f/50. The magnifications in Figure 16 is the same; the diffraction limited spot was an average of 55 μm in diameter. Figures 17(a) and 17(b) show the focused point for $\alpha_c = +15$ deg and $\beta_c = 0$. In Figure 17(a) the circle of least confusion produced with the lens apertured to f/20 is shown. In Figure 17(b) diffraction limited performance is obtained for an f/150 aperture. The dimension of the diffraction limited spot was approximately 200 μm.

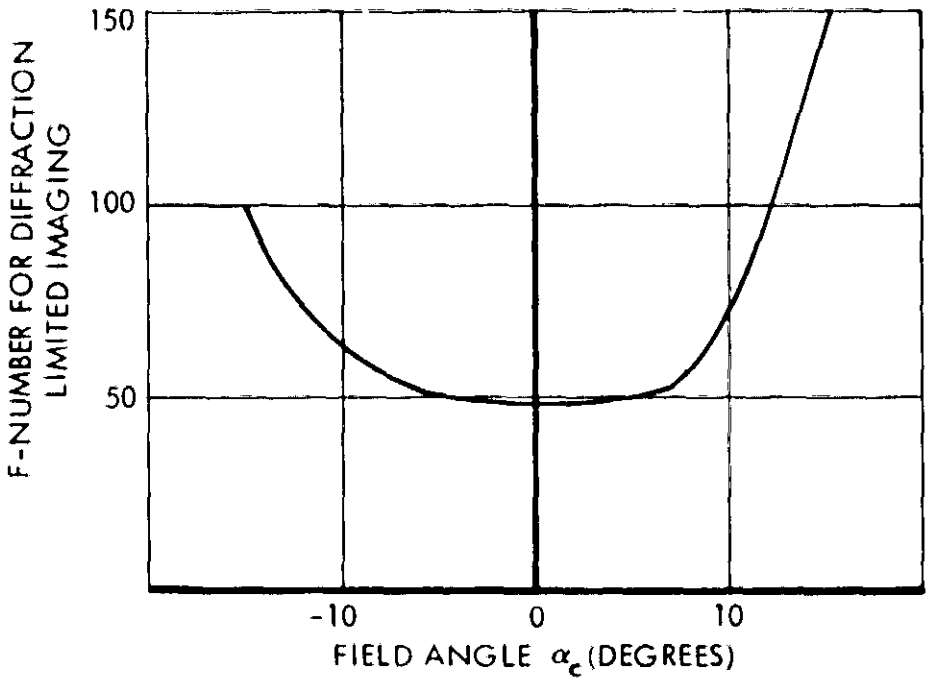

FIGURE 14. APERTURE PRODUCING DIFFRACTION LIMITED IMAGING AS A FUNCTION OF FIELD ANGLE α_c WITH $\beta_c = 0$.

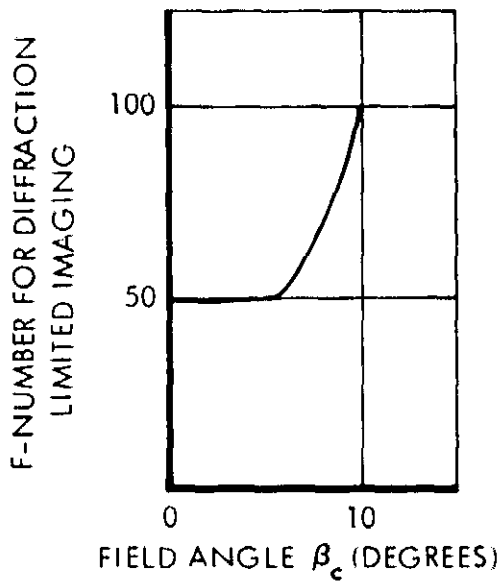

87974-15

FIGURE 15. APERTURE PRODUCING DIFFRACTION LIMITED IMAGING AS A FUNCTION OF FIELD ANGLE β_c WITH $\alpha_c = 0$.

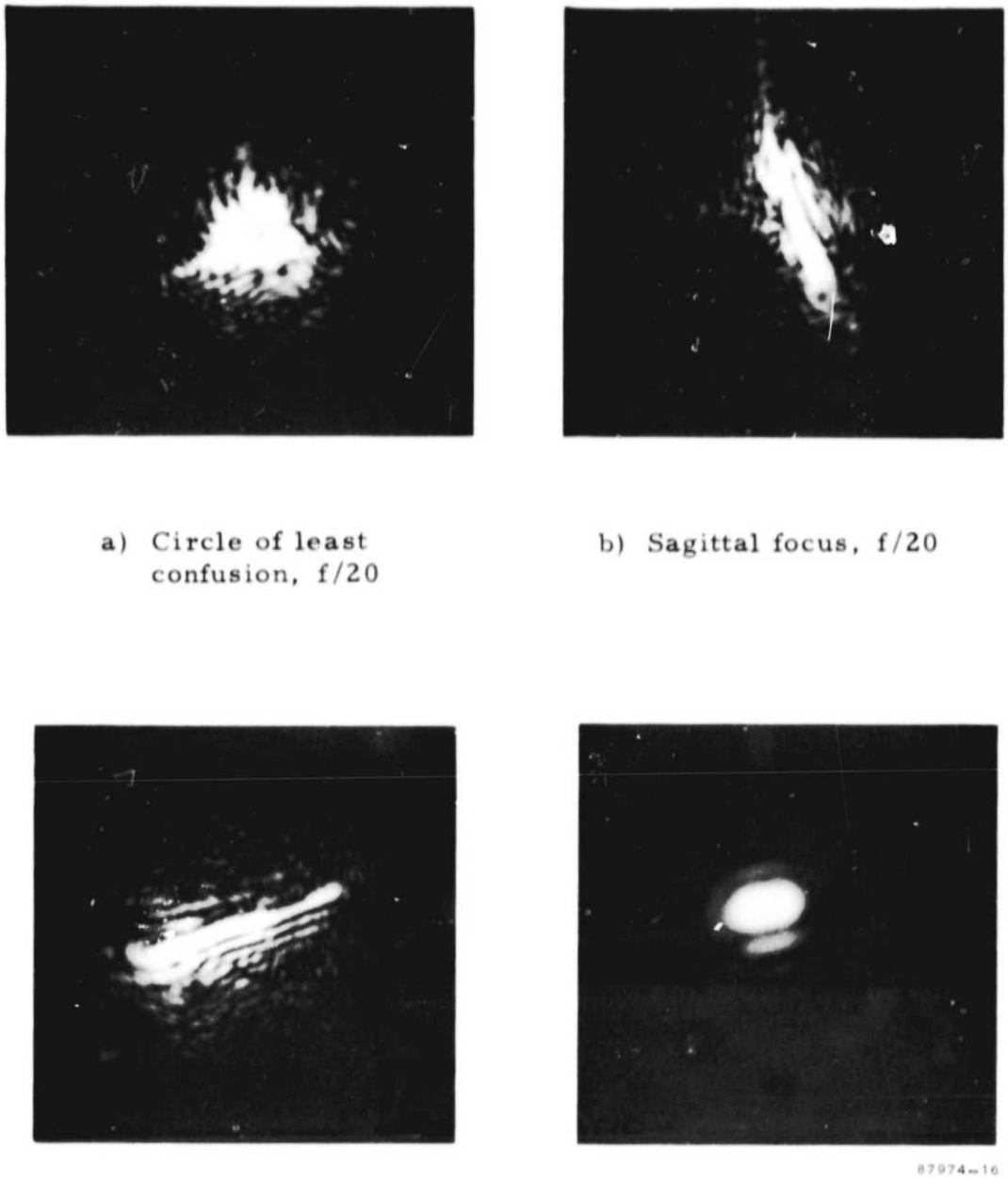

a) Circle of least confusion, f/20

b) Sagittal focus, f/20

c) Tangential focus, f/20

d) Diffraction limited, f/50

87974-16

FIGURE 16. POINT IMAGES FORMED BY WIDE ANGLE HOE SYSTEM FOR ON AXIS IMAGING AS A FUNCTION OF f-NUMBER

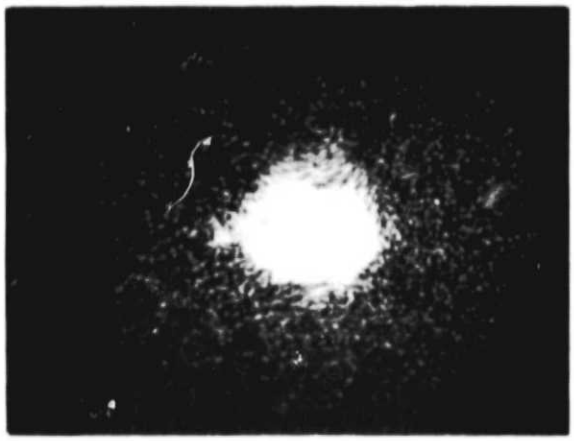

a) Circle of least confusion, f/20; $\alpha_c = +15^{\circ}$, $\beta_c = 0$

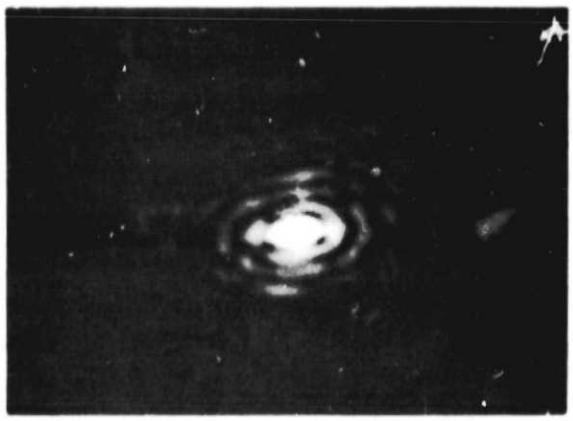

87974-17

b) Diffraction limited, f/150; $\alpha_c = +15^{\circ}$, $\beta_c = 0$

FIGURE 17. POINT IMAGES FORMED BY THE HOE SYSTEM FOR COHERENT, COLLIMATED ILLUMINATION INCIDENT AT $\alpha_c = +15$ DEG. AND $\beta_c = 0$

REFERENCES

1. M. Chang, Appl. Opt. 10, 2550 (1971).

2. L. H. Lin, Appl. Opt. 8, 963 (1969).

3. H. Kogelnik, B.S.T. J. 48, 2909 (1969).

SECTION IV

COMPUTER-GENERATED HOLOGRAPHIC OPTICAL ELEMENTS

4.0 INTRODUCTION

Since the introduction by Brown and Lohmann[1] of the concept of computer generated holograms in 1966, there has been considerable interest in the field of digital holography. The advantage of the computer-generated hologram is that one can create a hologram of a wavefront which exists only mathematically. With this motivation a substantial amount of research[1-13] has been dedicated to the coding of arbitrary wavefronts so that a particular computer graphic device could be optimally used to record synthetic holograms on film or similar recording materials. For obvious reasons the effects of quantization due to the computation performed by the computer and of the computer graphic devices on the recorded wavefront has also been investigated Applications of computer-generated holograms are three-dimensional displays, spatial filtering, and testing optical surfaces[18-22]. Because of fundamental limitations common to available computer graphic devices such as the Calcomp plotter and CRT displays, the problem of using computer holograms for high quality optical elements has not been investigated. McGovern and Wyant[21] used a computer-generated hologram to reconstruct an ideal spherical wavefront for testing optical surfaces. However, their paper did not give the details of how the wavefront was digitized, nor did they discuss the limitations on the wavefront due to the computer graphic device.

In this section we discuss a method for digitizing a wavefront, and how the wavefront is computed and recorded by a computer-controlled

laser scanner. We also discuss the limitations that a laser scanner imposes on the nature of the wavefront that can be recorded. We will show that the most important parameter in the digitizing and recording of a given wavefront is the space bandwidth product. The space bandwidth product of a wavefront recorded by using a laser scanner is limited by the space bandwidth product of the laser scanner. Finally, we suggest a method for increasing the space bandwidth product of the computer-generated hologram.

4.1 DIGITIZATION OF WAVEFRONTS

Before a given wavefront can be recorded on film or a similar recording material by a computer-controlled scanner, the wavefront must be digitized and used as the input to a computer program. The wavefront normally can come from experimental measurements or a mathematical expression. In this section we will deal with the digitization of wavefronts that can be written in analytical form. However, our results can provide insight about the number of data samples required to adequately describe any physical wavefront.

Suppose that a certain wavefront can be described analytically as

$$\phi(x) = \exp[j2\pi\theta(x)/\lambda] \quad \text{for} \quad |x| \leq A/2 \tag{1}$$

where $\theta(x)$ is the phase function in units of the wavelength λ and A is the hologram length. The wavelength λ is either the wavelength of the monochromatic light used to measure the phase function $\theta(x)$ or the wavelength that will be used later to reconstruct the computer-generated hologram. In Equation (1) we assume that the wavefront has variation only along the x-coordinate. It is a simple matter, of course, to extend our result to the two-dimensional case. Suppose that we have somehow recorded

$\Phi(x)$ on film and now illuminate the film with a collimated beam of coherent light. The incident light is diffracted by the phase structure $\theta(x)$. The local bending angle of the light passing through the film is given by

$$\psi(x) = \sin^{-1} \theta'(x) \tag{2}$$

where $\theta'(x)$ is the derivative of $\theta(x)$. The spatial frequency of the wavefront $\Phi(x)$ is equal to

$$\nu(x) = \frac{\sin \psi(x)}{\lambda} \approx \frac{\theta'(x)}{\lambda} \quad . \tag{3}$$

The bandwidth of the function $\Phi(x)$ can be defined as

$$B = 2\nu_{max} \tag{4}$$

where $\nu_{max} = \text{Max } |\nu(x)|$ and $|x| \leq \frac{A}{2}$.

We now consider the problem of taking samples of the wavefront $\Phi(x)$ and the means for adding a carrier frequency to the wavefront for recording on film. According to the sampling theorem, the sample values of $\Phi(x)$ are

$$\Phi_n = \Phi(n\Delta x) \tag{5}$$

where $\Delta x = 1/2\nu_{max}$. Because the wavefront $\Phi(x)$ is spatially limited, the number of data samples required to represent the wavefront is equal to

$$N = A/\Delta x \quad . \tag{6}$$

The parameter N is the space bandwidth product of the wavefront. Since $\Phi(x)$ is a complex function, it is necessary to convert $\Phi(x)$ into a real non-negative function before it can be recorded on film. This is accomplished

by putting the wavefront on a carrier frequency. However, this process unavoidably makes the space bandwidth product of the recorded signal greater than that of the wavefront $\phi(x)$.

We can determine the relationship between the signal to be recorded on the film and the sampled values of $\phi(x)$. Before doing so, we need the following definition for the discrete Fourier transform (DFT) of the sampled function ϕ_n. The DFT of $\{\phi_n\}$ is defined as

$$\tilde{\phi}_m = \sum_{n=1}^{N} \phi_n \exp(-j \frac{2\pi}{N} nm) \tag{7}$$

In order to put the function $\{\phi_n\}$ on a carrier, we compute the inverse DFT of $\{\tilde{\phi}_m\}$ as follows

$$\phi_k' = \frac{1}{N} \sum_{m=M/4}^{N+M/4} \tilde{\phi}_{m-M/4} \exp[j \frac{2\pi}{M} km] \tag{8}$$

$$\text{for } k = -M/2, \ldots, M/2 .$$

The parameter M is the total number of sample points to be recorded on the film. The shifting parameter $M/4$ will create a carrier frequency in the function $\{\phi_k'\}$. Because of the larger bandwidth required by having the signal on a carrier, the parameter M which is also the space bandwidth product of $\{\phi_k'\}$ must be larger than $2N$. By appropriate change of variables, we can rewrite Equation (8) as follows:

$$\phi_k' = \frac{1}{N} \exp(j \frac{\pi k}{2}) \sum_{m=1}^{N} \tilde{\phi}_m \exp(j \frac{2\pi}{M} km) \tag{9}$$

$$\text{for } k = -M/2, \ldots, M/2 .$$

By substituting Equation (7) into Equation (9) and rearranging terms, we obtain

$$\Phi_k' = \exp(j\frac{\pi k}{2}) \sum_{n=1}^{N} \Phi_n D(k,n) \tag{10}$$

where

$$D(k,n) = \frac{1}{N} \sum_{m=1}^{N} \exp[j\frac{2\pi m}{N}(\frac{N}{M}k-n)] \ . \tag{11}$$

The function $D(k,n)$ can be shown to be a Kronecker delta function. Therefore,

$$D(k,n) = \delta(\frac{N}{M}k-n) \ . \tag{12}$$

By substituting Equation (12) into Equation (10) we obtain

$$\Phi_k' = \exp(j\pi k/2)\, \Phi_{N/M\,k} \cdot \exp[j2\pi(\frac{k}{4} + \theta(\frac{N}{M}k\Delta x)/\lambda)] \ . \tag{13}$$

Finally, we take the real part of $\{\Phi_k'\}$, and add a constant bias to convert into a real nonnegative function. After this conversion, the sampled values of the signal to be recorded on film are equal to

$$F_k = \tfrac{1}{2} + \tfrac{1}{2}\cos 2\pi[\frac{k}{4} + \theta(\frac{N}{M}k\Delta x)/\lambda] \ . \tag{14}$$

If this signal is recorded on film with the spacing between samples equal to $\frac{N}{M}\Delta x$, we can reconstruct the wavefront $\Phi(x)$ by illuminating the film with a collimated beam of coherent light. From Equation (14) we note that we must sample the wavefront $\Phi(x)$ at a rate equal to $M/N\Delta x$ rather than $1/\Delta x$ in order to add a carrier frequency to the wavefront.

We can illustrate the technique just described by means of an example. Suppose that we want to generate a cylindrical wavefront with a focal length F and aperture A. The wavefront is given by

$$\Phi(x) = \exp\left[j \frac{2\pi}{\lambda} \theta(x)\right] \quad \text{for} \quad |x| < A/2 \tag{15}$$

where $$\theta(x) = \frac{1}{2\lambda F} x^2 .$$

By using Equation (3) we find that the spatial frequency as a function of x is equal to

$$\nu(x) = \frac{1}{\lambda F} x . \tag{16}$$

The maximum frequency occurs at the boundary of the function $\Phi(x)$ and is equal to $A/2\lambda F$. The bandwidth B of $\Phi(x)$ is therefore equal to $A/\lambda F$ and the sampling interval Δx is equal to $\lambda F/A$. From Equation (6) the space bandwidth product is equal to

$$\begin{aligned} N &= A^2/\lambda F \\ &= FR^2/\lambda \end{aligned} \tag{17}$$

where R is the aperture ratio A/F. For $\lambda = 0.6328$ μm, $F = 1000$ mm, and $R = .05$, the space bandwidth product is calculated to be 3950. This indicates that we need 7900 samples to record this wavefront on film. Moreover, the spacing between samples $N\lambda/MR$ is equal to 12.8 μm.

Substituting $\theta(x)$ in Equation (15) into Equation (13) we obtain

$$\Phi_k' = \exp\left\{+j2\pi\left[\frac{k}{4} + \frac{N^2}{2M^2}\left(\frac{\lambda F}{A^2}\right)k^2\right]\right\} . \tag{18}$$

By replacing $A^2/\lambda F$ with N, Equation (18) becomes

$$\Phi_k' = \exp\left[+j2\pi\left(\frac{k}{4} + \frac{Nk^2}{2M^2}\right)\right] . \tag{19}$$

It is interesting to note that in generating a spherical wavefront, only the parameter N and the spacing Δx between samples are required to characterize the wavefront.

4.2 LASER SCANNER CONSIDERATION

The important parameters of a laser scanner are the scanning spot size and the total number of spots that can be recorded on film. We now show by way of example how a laser scanner limits the recording of wavefronts when the computer technique previously described is used. For example, if we want to record a spherical wavefront with a laser scanner on film, it can be shown that the F-number of the spherical wavefront is directly related to the center spacing of the spots scanned on film by the scanner. From previous analysis, the sampled wavefront for a spherical wave is given by

$$\Phi_k = \exp\left[j \frac{\pi N}{M^2} k^2\right] . \tag{20}$$

Suppose that we record this sampled wavefront on film using a center spacing Δx between the scanner spots. The complex wavefront recorded on film can be written as

$$\Phi(x) = \sum_{k=1}^{M} \exp\left(j \frac{\pi N}{M^2} \frac{x^2}{\Delta x^2}\right) \delta(x - k\Delta x) \tag{21}$$

where $\delta(x)$ is a Dirac delta function. By comparing the form of $\Phi(x)$ to that of a spherical wave, we find that the focal length of $\Phi(x)$ is

$$F = M^2 \Delta x^2 / \lambda N . \tag{22}$$

Since the aperture of the spherical wavefront is equal to $M\Delta x$, the F-number of the spherical wavefront is simply

$$\text{F-number} = M\Delta x/\lambda N \quad . \tag{23}$$

As we discussed in the previous sections, the condition on M is that it must be equal to or larger than $2N$. As a result, the smallest F-number achievable with a center spacing of Δx is

$$\text{F-number} = 2\Delta x/\lambda \quad . \tag{24}$$

For example, if the center spacing Δx is 2 μm and λ is 0.5 μm, the smallest F-number achievable is 8. Because the wavefront is mixed with a spatial carrier frequency, the modulation of the fringe pattern recorded on film is provided by the adequate separation of the scanned spots. Therefore, to obtain a f/8 wavefront, we need a spot size of less than 2 μm. Because the center spacing between spots in this case is about 4λ, the jitter of the scanned positions must be less than λ to reduce the possibility of having aberrations in the recorded wavefront.

Generally there is no need for real time generation of optical elements. Therefore, a relatively slow, straightforward recording technique can be used. A low-speed scanner, using an electro-optic modulator driven by the D/A converted output of a small computer appears to be adequate.

4.3 COMPUTER CONSIDERATION

The general procedure in using the computer and the laser scanner to record a wavefront on film consists of two steps. First the wavefront has to be digitized (scanned line by scanned line). The data obtained from each scanned line is then stored on magnetic tapes. Then a different computer program reads out the data from tape and directs the scanner to record the wavefront on film. This approach has the advantage that the digitization of the wavefront can be done on a general purpose

computer, while the scanner is controlled by a relatively small computer. The computation time for digitizing the wavefront depends on the complexity of the wavefront. If the information about the wavefront is given in the form of an interferogram, then more computation is necessary. Because the major task of computing the wavefront is done on a general purpose computer, the demand on the small computer is rather minimal. In using our laboratory scanner to record data on film, the DC motor in the scanner drives the film plates continuously from one end to the next. Therefore, it is necessary to have all the points along a scanned line stored in the core memory. In the case of our laboratory computer, this means that each scanned line can not have more than 4096 points. This restriction is not necessary if the scanner is designed to act like an incremental plotting device.

REFERENCES

1. B. R. Brown and A. W. Lohmann, "Complex Spatial Filtering with Binary Masks", Appl. Opt., Vol. 5, No. 6, June 1966, pp 967-969.

2. B. R. Brown and A. W. Lohmann, "Computer-generated Binary Holograms", IBM J. Res. Develop., Vol. 13, No. 2, Mar. 1969, pp 160-168.

3. J. P. Waters, "Holographic Image Synthesis Utilizing Theoretical Methods", Appl. Phys. Lett., Vol. 9, Dec. 1, 1966, pp 405-407.

4. J. P. Waters, "Three Dimensional Fourier-Transform Method for Synthesizing Binary Holograms", J. Opt. Soc. Amer., Vol. 58, Sept. 1968, pp 1284-1288.

5. J. P. Waters and F. Michael, "High Resolution Images from CRT-Generated Synthetic Holograms", Appl. Opt., Vol. 8, Mar. 1969, pp 714-715.

6. A. W. Lohmann and D. F. Paris, "Binary Fraunhofer Holograms Generated by Computer", Appl. Opt., Vol. 6, Oct. 1967, pp 1739-1748.

7. T. S. Huang and B. Prasada, "Considerations on the Generation and Processing of Holograms by Digital Computers", MIT/RLE Quar. Prog. Rep. 81, Apr. 15, 1966, pp 199-205.

8. Y. Ichioka, M. Izumi, and T. Suzuki, "Halftone Plotter and its Applications to Digital Optical Information Processing", Appl. Opt., Vol. 8, 1969, pp 2461-2471.

9. Y. Ichioka, M. Izumi, and T. Suzuki, "Scanning Halftone Plotter and Computer-Generated Continuous-tone Hologram", Appl. Opt., Vol. 10, Feb. 1971, pp 403-411.

10. S. C. Keeton, "A Sampled Computer-Generated Binary Hologram", Proc. IEEE (Lett.), Vol. 56, Mar. 1968, pp 325-327.

11. W-H. Lee, "Sampled Fourier-Transform Hologram Generated by Computer", Appl. Opt., Vol. 9, Mar. 1970, pp 639-643.

12. W-H. Lee, " Filter Design for Optical Data Processors", Pattern Recog., Vol. 2, May 1970, pp 127-137.

13. L. B. Lesem, P. Hirsch and J. A. Jordan, Jr., "The Kinoform: A New Wavefront Reconstruction Device", IBM J. Res. Develop., Vol. 13, Mar. 1969, pp 150-155.

14. R. A. Gabel and B. Liu, "Minimization of Reconstruction Errors with Computer-Generated Binary Holograms", Appl. Opt., Vol. 9, May 1970, pp 1180-1191.

15. J. W. Goodman and A. M. Silverstri, "Some Effects of Fourier Domain Phase Quantization", IBM J. Res. Develop., Vol. 14, Sept. 1970, pp 478-484.

16. W. J. Dallas, "Phase Quantization--A Compact Derivation", Appl. Opt., Vol. 10, No. 3, Mar. 1971, pp 673-674.

17. W. J. Dallas, "Phase Quantization in Holograms--A Few Illustrations", Appl. Opt., Vol. 10, No. 3, Mar. 1971, pp 674-676.

18. B. R. Brown, A. W. Lohmann, and D. P. Paris, "Computer Generated Optical-Matched Filtering", Opt. Acta, Vol. 13, 1966, p 377.

19. A. W. Lohmann and D. P. Paris, "Computer Generated Spatial Filters for Coherent Data Processing", Appl. Opt., Vol. 7, Apr. 1968, pp 651-655.

20. A. W. Lohmann, D. P. Paris, and H. W. Werlich, "A Computer-Generated Spatial Filter Applied to Code Translation", Appl. Opt., Vol. 6, June 1967, pp 1139-1140.

21. A. J. MacGovern and J. C. Wyant, "Computer-Generated Holograms for Testing Optical Elements", Appl. Opt., Vol. 10, Mar. 1971, pp 619-624.

22. H. J. Caulfield and S. Lu, "Applications of Computer-Generated Holograms", in the Applications of Holography, New York: Wiley-Interscience, 1970, ch. 10.

SECTION V
NEW TECHNOLOGY

After a thorough review of the work performed under the terms of this contract, we find that no new innovation, discovery, improvement or invention has resulted.

SECTION VI

FINANCIAL STATUS

A. Expenditures to Date: $53,216

B. Funding Required For Completion: $53,216

C. Problem Areas: . . . . . None

APPENDICES

We have included in this report two studies by Electro-Optics Operation personnel describing related work in the area of holographic optics. Appendix A summarizes experimental data relevant to the fabrication of large diameter, single component HOE intended for use as collimators. Appendix B provides an example of possible applications of volume phase gratings. In this particular case a volume phase grating is used as a Bragg-effect wavelength selector in a tunable dye laser.

APPENDIX A

LARGE APERTURE HOLOGRAPHIC OPTICAL ELEMENTS*

A. 1 INTRODUCTION

In this appendix we summarize an investigation of problems related to the fabrication of large aperture holographic optical elements. Although the properties of a hologram are invariant with size, this is not true with regard to its construction. That is, large holograms intended for imaging applications are significantly more difficult to construct than small holograms. High quality light-sensitive materials and optical quality substrates of large area are minimum requirements. The substrate must be coated with light-sensitive recording material in the most uniform way possible to avoid aberrations and other imaging defects. Over small areas this is not difficult, however, it is not a trivial task for holographic elements 25 cm in diameter or larger.

We limit our discussion to the fabrication of reflective elements. The specifications are a 25 cm diameter, a focal length of 1.2 meters, and a bending factor of 2.2. Two approaches are possible: a reflection hologram of the Lippmann-Bragg type or a planar reflection hologram. For many applications the latter is potentially more useful, especially when metal or dielectric reflective coatings and blazing are considered. Obvious applications come to mind for optical systems operating in the UV or IR spectrum. The best recording medium in terms of resolving power and diffraction

* R. G. Zech and L. M. Ralston, Final Report 6317-F (Prepared for Dr. J. Latta, ERIM, September 1973).

efficiency is a high resolution photoresist. Several are available; they will be described subsequently.

We have divided our summary into a number of areas. The most important are recording materials, substrate fabrication, coating techniques, and hologram construction. A discussion of the main results of the study follows.

A. 2 RECORDING MATERIALS

The fabrication of high quality holographic optical elements (HOE) requires exceptionally well-qualified recording materials. Not only must the recording media be capable of good holographic performance, but must also possess favorable physical properties and chemical stability. The latter is of particular importance for large diameter HOE. From previous experimental work related to the present study, it was clear that only a few recording materials would be suitable. Although we eventually chose a photoresist for constructing the HOE because a reflective element was constructed, we surveyed a number of potentially useful recording materials. The main properties and characteristics of the better candidate light-sensitive materials for HOE applications are summarized in tabular form (Table 5).

The best photoresists available for holographic recording are Shipley AZ 1350 and Horizons Research LHS7. Shipley AZ 1350 is widely used in the microelectronics industry. It is UV-blue sensitive with a resolving power of about 1500 cycles/mm (70% response). Maximum reported efficiency for plane wave gratings is 30%. Processing involves a liquid development and postbaking. The Horizons Research LHS7 photoresist is new. It is characterized by a relatively high orthochromatic exposure

TABLE 5

CANDIDATE HOE RECORDING MEDIA

Recording Material	Type[a]	Speed[b] (mJ/cm²) at 488 nm	R. P.[c] (cycles/mm)	Spectral Response	D. E.[d] (%)	SNR[e] (dB)	Processing Req'ts.
Dichromated Gelatin	VP	100	> 3000	blue-green	> 90	> 25	Chem.
Acrylate Photopolymer-(DuPont)	VP	10	> 2000	UV blue-green	> 50	> 25	None
Bleached Photo. Emulsion (Kodak 649F)	PP VP	.01	> 3000	UV visible	> 30	> 20	Chem.
Photoresist	PP						
a) Shipley AZ1350		10^4	> 1500	UV blue	> 25	> 15	Chem.
b) Horizons LH57		5	> 1000	UV blue-green	> 25	> 20	Heat
Photodegradable Thermoplastics	VP	10^3	> 3000	blue-green	> 60	> 30	None
Photoplastics	PP	.01	> 1000	UV visible IR	> 20	> 15	Heat

[a] VP = volume phase
PP = planar phase

[b] Speed = exposure for maximum diffraction efficiency.

[c] R. P. = resolving power

[d] D. E. = diffraction efficiency (ratio of diffracted light to incident light for a plane wave grating).

[e] SNR = signal/noise ratio. All data for a fixed packing density and beam ratio.

sensitivity, a resolving power of 800 cycles/mm (70% response), and a maximum diffraction efficiency of 31%. Cosmetic quality is very good. A unique aspect of this photoresist is that it is completely developed and fixed with heated air (at 160 ° C for 90 seconds).

A.3 FABRICATION STUDY

A.3.1 Substrate Fabrication

There is a limited choice of substrate materials. We considered glass and plastic. Plastic was rejected because of surface adhesion problems, and because it is fairly difficult to obtain a large plastic sheet with a good optical surface. The most practical choice was a plate glass substrate with dimensions of 27.5 x 27.5 cm^2 and 2.54 cm thick. It was ground and polished to $\lambda/4$ on the front surface and lapped and felt polished on the back surface. Edges were beveled, ground, and polished. The work was done by J. Vanden Broeck at the McDonald Douglas Electronics Corporation (St. Charles, Mo.) optical fabrication shop for a total price of $550.

We should point out that selection of a substrate is determined mainly by optical figure requirements. In general the substrate thickness increases proportionately with surface quality. However, some glasses are better (and more expensive) than others in terms of figuring. A good grade of quartz, e.g., T14 Optosil 3 (Amersil Co.), is recommended because of superior dimensional stability that allows a 30% decrease in thickness (and also weight.

A.3.2 Surface Adhesion

The adhesion to glass of most photoresist materials is generally poor. The large area of the HOE compounded the problem. We concluded at the start of the program that a substratum layer was required. Unfortunately, a subbing compound was not available from the manufacturers of the photoresists. We performed a literature search, but discovered that the most effective (and nonscattering) subbing chemicals were proprietary to the large photographic film manufacturers. The most attractive alternative remaining was to develop a suitable technique for cleaning the glass substrate. As is well known, the adhesive properties of a surface are enhanced by thorough cleaning.

The procedures we evolved are elementary, but effective. Two cases were of interest: (1) previously uncoated substrates, and (2) previously coated substrates from which the photoresist layer was stripped. To clean new substrates we recommend the following steps:

1) airknife off dust and large surface particles;
2) rinse in a solvent consisting of equal parts of methyl alcohol, chloroform, and benzene;
3) wash in a multicomponent detergent, e.g., Microclean; and
4) triple rinse in distilled water and free air dry.

Cleaning previously coated substrates was complicated by the residue of the stripped photoresist layer. As a consequence, a more vigorous cleaning technique is required. We found by trial and error that the following procedure is effective for the Horizons Research photoresist:

1) Bathe in Horizons Research photoresist developer.
2) Rinse in warm methylene chloride for 30 minutes.
3) Scrub in fresh methylene chloride with a teflon pad.
4) Scrub in a multicomponent detergent with a teflon pad.
5) Triple rinse in distilled water and free air dry.

Just prior to coating the photoresist layer, we discovered that two other steps were necessary. First, we baked the substrate at 150°C for one hour to remove surface moisture. A high wattage air gun (rated to 500°C) is also effective for this task. After cooling to room temperature and transporting to the clean room, the substrate was bathed in filtered dry nitrogen. These steps are of particular importance under conditions of high relative humidity.

When the procedures just outlined are used, good adhesion between the photoresist layer and the glass substrate are consistently obtained. We note, however, that this assumes that the photoresist layer is continuous, and that the edges of the substrate are sealed. When these conditions are not realized, the coating can be damaged, as will be discussed later.

A.3.3 Coating Techniques

Coating a 27.5 cm square glass substrate with various photoresist solutions required the investigation of numerous coating techniques. Because of obvious uniformity and cosmetic quality requirements, only three techniques appeared feasible. They were spin-coating, dip-coating, and gravity-flow coating. Each has advantages and disadvantages. For example, spin-coating was feasible with modification to the spinning

apparatus. However, the large mass of the glass substrate prevents sufficient acceleration to spinning speed. As a result, nonuniform coatings are obtained.

High quality coatings were obtained on small substrates by dip-coating. The extension of this technique to 27.5 cm square substrates is not possible for three reasons. First, the thickness of the photoresist layer is found to vary in a nonlinear way (a linear wedge is acceptable). The height profile of the photoresist layer is linearly wedged (approximately) over the first 75 percent of the length of the substrate but then increases more rapidly. This is for substrates having dimensions of 2 cm x 3 cm. We concluded that the same characteristics would apply to the larger substrates. Second, a large volume of photoresist is required to be maintained free of dust and moisture. A significantly larger than average cleanbox is needed for this purpose in order to also allow for withdrawing the entire length of the substrate from the coating solution. Finally, the coated layer must dry in a solvent atmosphere to insure a smooth, uniform photoresist layer. The solvents used in both the Shipley and Horizons Research photoresists have insufficient room temperature vapor pressure for this purpose.

Our preliminary investigation established that gravity-flow coating is the only feasible technique. Although there are a number of ways to implement this method, we describe ours to illustrate some of the problem areas. The details of our approach are outlined in what follows.

The gravity-flow setup consisted of a 30 cm^2 granite table flat to 0.5 μm, a 2.5 cm thick tripoded surface plate for leveling the granite slab, an aluminum casting frame, and an airtight cover to provide a solvent atmosphere for slow drying. The granite slab and leveling plate were

located in a vibration free area to minimize surface perturbations. The casting frame, as shown in Figure 18a, was made from four 27.5 cm strips of 0.32 cm aluminum. The corners are cut to 45° and the strips were bent along the center to approximately 45°. When taped to the substrate, the frame draws up the solution by capillary action forming an edge of zero thickness just inside the frame, as shown in Figure 18b.

A 10 cm x 12.5 cm substrate coated by this method was supplied by C. Leonard of the Environmental Research Institute of Michigan. It was tested with a Leitz reflecting interference microscope for surface uniformity. Ignoring edge effects, we found a maximum thickness variation of less than 0.225 μm. This test showed that gravity flow casting can be used to coat substrates with sufficient uniformity. That is, the recording material will cause a random wavefront aberration of less than $\lambda/2$ over the 25 cm aperture of the HOE.

The airtight cover had a dual purpose; to keep out light and dirt, and to provide a solvent atmosphere. If the coated substrates are allowed to free-air dry, the top layer of the photoresist which is in direct contact with the atmosphere dries first. Then as the lower layers dry, the solvent must evaporate through the top surface layer; this causes a rippled surface (orange peel). Substrates allowed to dry entirely in a solvent atmosphere in general have good surfaces, but can take up to eight hours to completely dry. The airtight cover was used to provide a compromise between these extremes. That is, the photoresist solution is flowed on the substrate and the cover is tightly closed for one hour to allow the solution to spread uniformly. The cover is opened briefly to vent the solvent atmosphere, and then closed. The rate of drying is controlled by the frequency with which

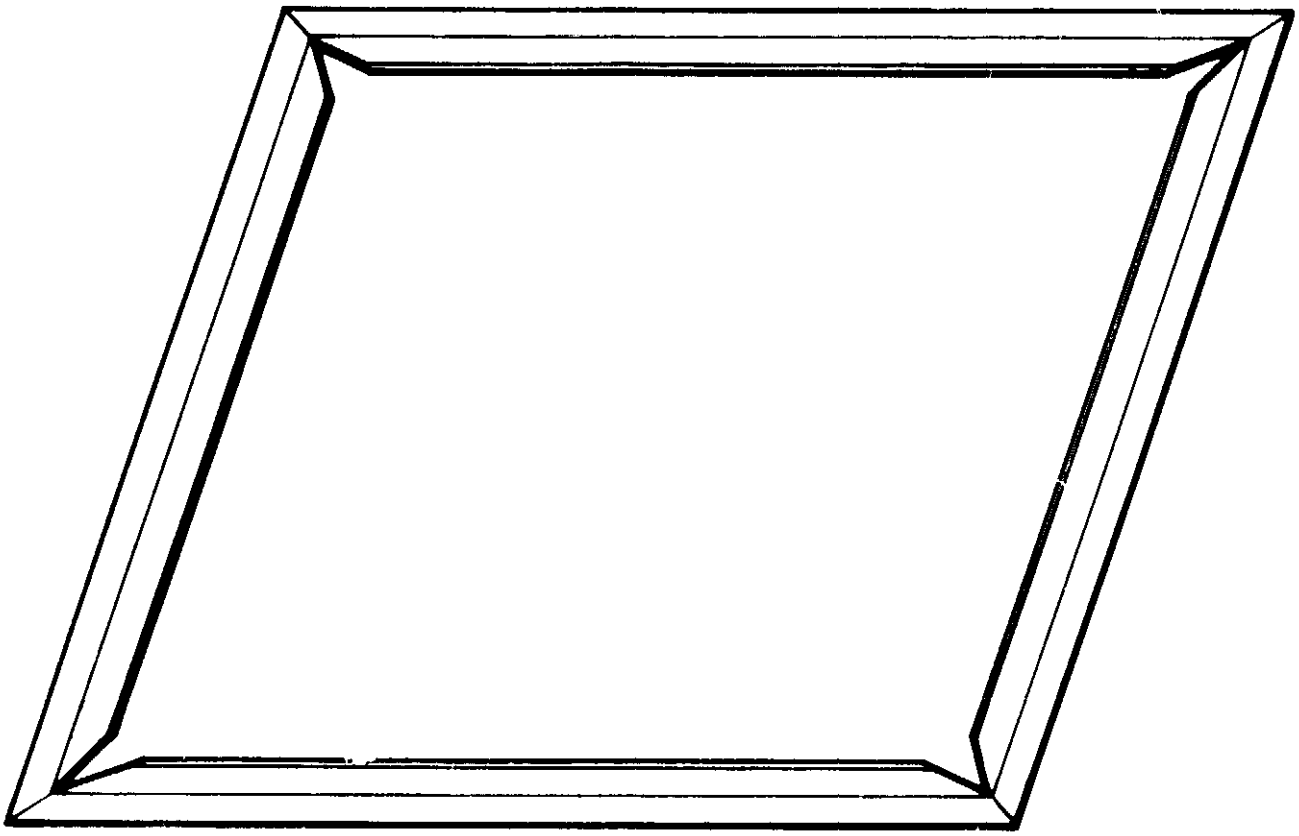

FIGURE 1a

87554-2

FIGURE 1b

FIGURE 18. CASTING FRAME (a) AND PHOTORESIST (b) FOR GRAVITY FLOW CASTING.

the solvent atmosphere is vented. If the photoresist is allowed to dry too fast, orange peel forms; too slowly and the plate is covered with dust and other artifacts.

The first coatings were cast in a photographic dark room using Shipley AZ 1350 photoresist. In order for the resist to uniformly spread over the entire substrate, it was diluted to a concentration of one part AZ 1350 to eight parts methyl ethyl ketone (MEK). On the order of 15 cc of the photoresist solution was flowed in the center of the substrate and dried completely in a solvent atmosphere. The resultant coatings were uniform but cosmetically poor due to a large amount of dust particles. We used internal filtered air (fan-driven) to reduce the dust particle concentration; this proved to be helpful, but insufficient. The entire casting apparatus was then moved to a clean room environment, and set up under a laminar flow hood. Plates fabricated in the clean room dried with a lower dust particle concentration than those cases in the dark room. However, cosmetic quality remained below acceptable standards. We reached the conclusion that Shipley AZ1350 has a natural affinity for airborne particulate matter.

The evaluation of the Horizons Research photoresist was initiated in the clean room environment. We found that diluting one part of HR photoresist with five parts solvent provided a uniform coating of approximately one micron thick. The coatings were significantly cleaner than coatings made with Shipley AZ1350. In addition, we found that coatings made with the Horizons Research photoresist were more consistent. However, the Horizons Research photoresist required a much longer drying time than the Shipley photoresist (drying time is a critical factor in providing good surface). Nevertheless, we decided that an increased drying time was

a favorable tradeoff in order to gain acceptable cosmetic quality and consistency. Therefore, we selected Horizons Research photoresist for fabrication of the HOE.

In addition to the problems caused by dust and other airborne particles, we encountered two more subtle problems. The first was glass warpage. When a large glass substrate is fabricated to a specified optical quality (in this case $\lambda/4$ surface flatness) there can be differences between neighboring areas that require a precision optical flat of comparable area to defect (in the present case this implies a flat that is $\lambda/20$ and $25\sqrt{2}$ cm in diameter). The second was stability. We found that the level of the substrate could be significantly changed for example, by foot traffic in the region of the clean area. Both of these problems resulted in low quality photoresist layers. Our solution to the first problem consisted of weighting the casting frame to compensate for the warpage. This was done with aluminum blocks. We avoided stability problems by casting during evening and weekend hours when activity in the clean room area was at a minimum. A better solution would be a small floating table, e.g., mercury supported.

Finally, we again stress the problems caused by particulate matter. The photoresist solution can be purged by microfiltering prior to use. Airborne contaminants must be avoided by the use of a laminar airflow in a clean room environment. Our study indicated that temperature, relative humidity, drying time, and photoresist solvent (including diluent) are also important factors.

A.3.4 Hologram Recording

The hologram recording setup is shown in Figure 19. It consists of two point sources located at 2 m and 0.75 m distance from the center of

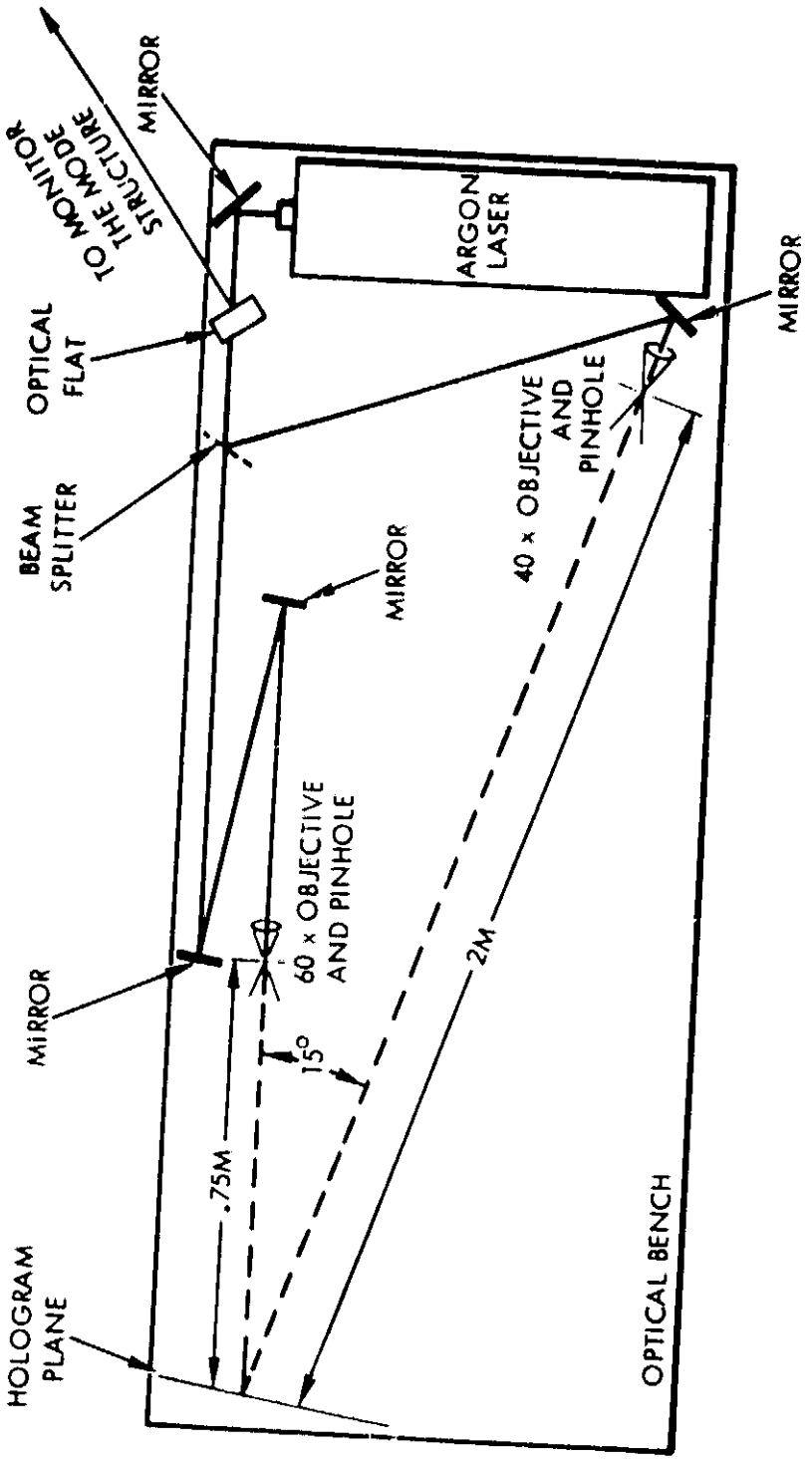

FIGURE 19. EXPERIMENTAL SETUP USED FOR THE LARGE DIAMETER HOE CONSTRUCTION.

the hologram recording plane. The angular separation, measured with a goniometer, is 15°. The plateholder is oriented so that the fringes are normal to the surface of the recording material.

In order to insure spherical waves of uniform intensity over the entire aperture of the HOE, we expanded each beam to an area twice the diagonal of the glass substrate. This significantly reduced the laser power density available for exposure. Total irradiance at the hologram recording plane was only 10 $\mu W/cm^2$ using a 2W argon laser operating at 488 nm in a single transverse and longitudinal mode (output was 300 mW). Exposure time was 12 minutes; this indicates the value of high exposure sensitivity. If Shipley AZ1350 had been used, more than 8 hours of exposure would be needed.

Prior to hologram recording, an optical black lacquer was applied to the back of the coated substrate. After exposure, the holograms were stripped of the antihalation backing, and then processed with a hotplate (100°C) and an airgun (160°C). The hotplate was used to heat the substrate and thus to avoid thermal shock when the airgun was applied to the photoresist layer for development.

A.4 COMPLETION OF FABRICATION

After processing, the best holograms were aluminized and silicon monoxide overcoated to produce reflective elements. This work was done at the optical facilities of the McDonnell Douglas Electronics Corporation (St. Charles, Mo.). The price was $51 per hologram.

As part of the preparation for aluminizing, the photoresist layer was cleaned with dry air to remove dust particles and then wash-ed

with a detergent and water. All holograms except one (unfortunately the best HOE) survived this treatment. It was later discovered that one corner of the substrate of the damaged HOE did not seal. This caused a section of the photoresist to lift off the substrate. A small scratch permitted the same phenomenon to occur near the center of the HOE. This was unfortunate because the damaged HOE was of high quality otherwise, and also of high efficiency.

To complete fabrication, each HOE was painted on the back surface with an optical black lacquer. The front surface of the HOE was covered with a black aperture 25 cm in diameter. The aperture is not necessary, but serves to define the usable area of the HOE (the edges are of poor quality) in an obvious way. A photograph of a completed HOE is shown in Figure 20.

A.5 CONCLUSIONS

The fabrication of large aperture HOE is feasible. In the limited context of our investigation we sought to isolate problem areas. A great number were discovered. However, none were found to be insoluble. But it is clear that very exacting procedures are required if optimum results are to be obtained. In particular, we emphasize the need for high quality substrates, a superior clean room facility, and a fairly sophisticated coating apparatus.

We find no reason to believe that large aperture HOE could not be produced in large numbers. In fact, many of the problems we encountered were those of scale, and would normally be absent in a

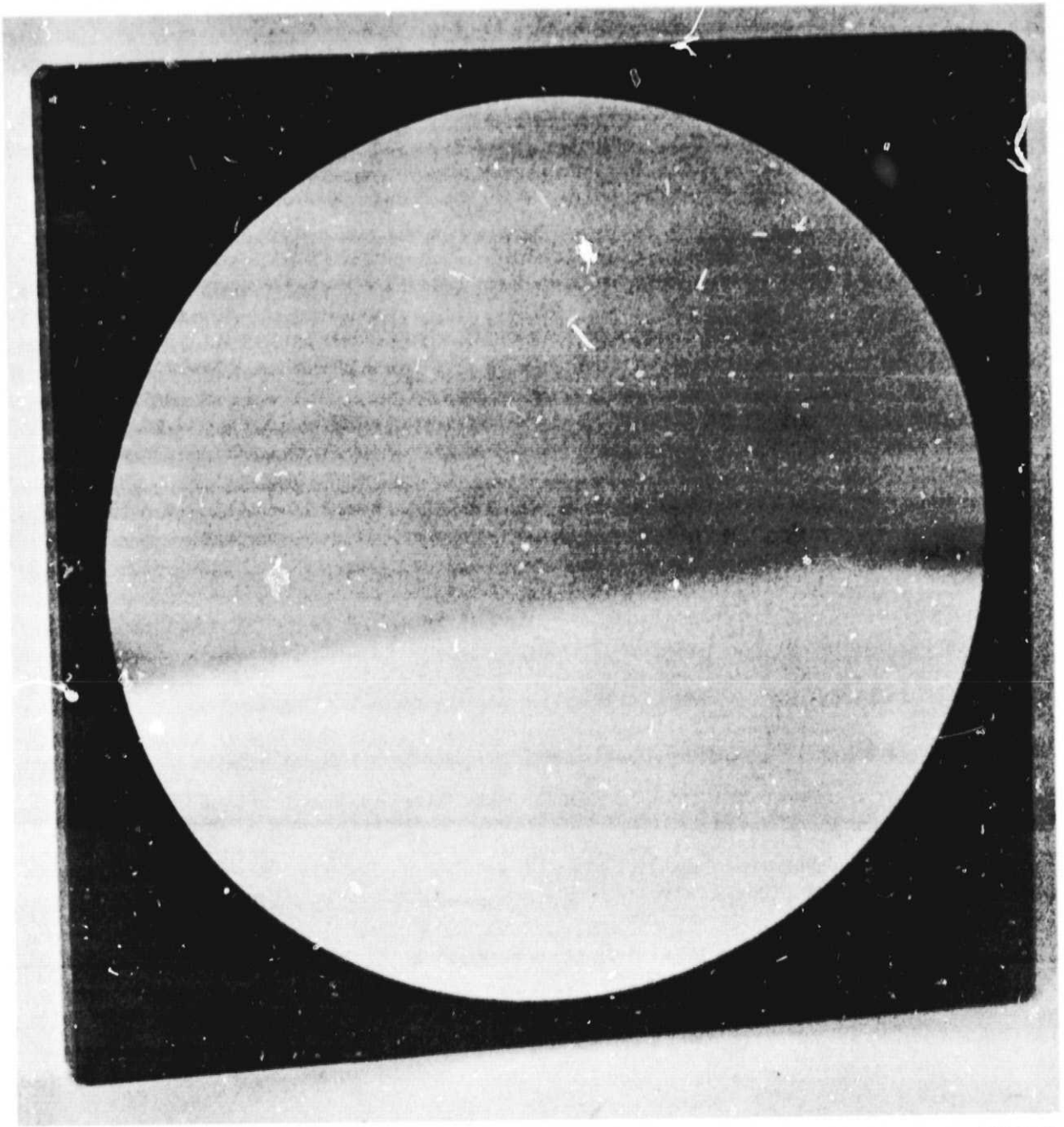

87974-18

FIGURE 20. LARGE APERTURE HOE AFTER FINAL FABRICATION AND PACKAGING

production facility. Once procedures were optimized, large aperture HOE could be fabricated on a mass production basis.

A.6 RECOMMENDATIONS

Further study of fabrication techniques is warranted. The major areas are substrates (materials, subbing, optical figure, etc.), coating techniques (optimization of the gravity flow method), and overcoating (metal versus dielectric and also surface preparation). Each area represents a phase of construction that merits optimization if high quality HOE are to be produced that are competitive with conventional optics.

APPENDIX B

AN APPLICATION OF HOLOGRAPHIC GRATINGS: SIMULTANEOUS MULTIPLE OPERATION OF A TUNABLE DYE LASER*

B.1 INTRODUCTION

We present a simple and convenient scheme for operating a tunable pulsed dye laser at a number of selected wavelengths simultaneously. Two wavelengths operation was achieved previously by Taylor, et al[1] and by Zalewski and Keller[2]. More recently, Pilloff[3] demonstrated a scheme in which the two wavelengths are decoupled by forcing the dye laser to produce them with mutually orthogonal polarization. Unlike the above techniques, no intracavity elements are needed in our scheme, so that insertion losses are avoided. Furthermore, more than two wavelengths can be obtained, and these wavelengths can have the same polarization.

B.2 EXPERIMENTAL SETUP

The experimental setup is shown schematically in Figure 21. Pulses from a nitrogen laser are focused by a cylindrical lens (L) into the dye cell (D), in a transverse pumping configuration. The wavelength selectors G_1 and G_2 are holographic gratings with spatial frequencies of about 3000 lines/mm, constructed as described by Kogelnik, et al[4]; each grating was sandwiched between a glass substrate and a reflecting mirror (~ 90% reflectivity across the visible). The output coupler (M)

---

* Contributed by Dr. A. A. Friesem (on academic leave to the Weizmann Institute, Rehovot, Israel); submitted to Applied Physics Letters with U. Ganiel and G. Neumann.

is a broadband dielectrically coated plane mirror with approximately 40% reflectivity. An important feature of the arrangement is the shortness of the cavity which is advantageous in short pulse operation. Typical distances are M to G_1, 7 cm; G_1 to G_2, 4 cm; and a dye cell of an overall length of 4 cm with 15 mm pumped region.

B.3 OPERATION

The operation of our device is described with reference to Figure 21. The grating G_1 is first oriented so that some particular wavelength, say λ_1, is incident at the Bragg angle, and hence radiation at this wavelength is reflected back into the laser cavity. Simultaneously, some other spectral component of the broadband fluorescence of the dye, say λ_2, will not satisfy the Bragg condition, so that the grating-mirror sandwich structure G_1 will simply reflect it toward G_2. If now G_2 is oriented to satisfy the Bragg condition for λ_2, feedback at λ_2 is obtained. Radiation at the two lasing wavelengths passes through the active medium along the same path, and the output beam contains both λ_1 and λ_2 simultaneously. Note that once λ_1 is selected by a specific orientation of G_1, radiation at other wavelengths is non-dispersively reflected toward G_2; λ_2 can thus be tuned across the gain band without changing the alignment of G_1. However, radiation at wavelengths close to λ_1 is partially diffracted by G_1, so that it arrives at G_2 with a loss of intensity. In particular the diffracted intensity of the holographic grating has a spectral half power bandwidth $(2\Delta\lambda_{1/2})$ given by[4,5]

$$2\Delta\lambda_{1/2} = [\lambda^2(n^2 - \sin^2\theta)^{1/2}]/2d\sin^2\theta \qquad (1)$$

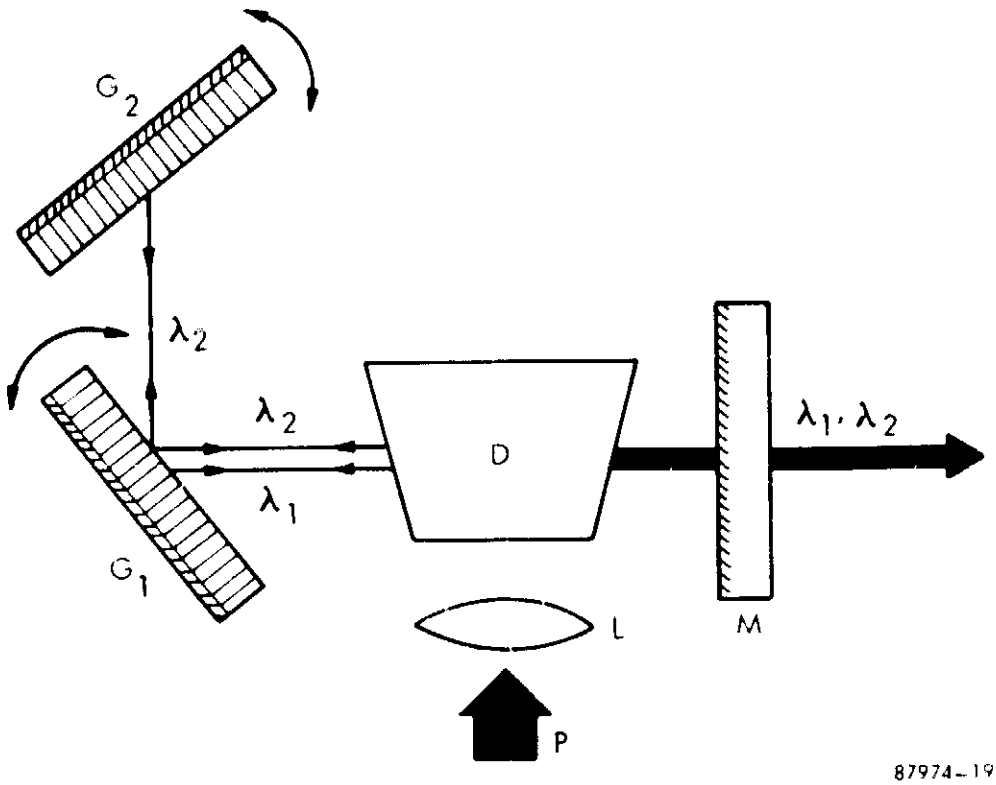

FIGURE 21. SCHEMATIC DIAGRAM OF EXPERIMENTAL ARRANGEMENT. P-PUMP BEAM, L-CYLINDRICAL LENS, D-DYE CELL, M-OUTPUT MIRROR. G_1 AND G_2 - HOLOGRAPHIC WAVELENGTH SELECTORS.

where θ is the angle of incidence, d is twice the thickness of the grating, and n is the index of refraction of the grating medium. In our experiments, where $\theta \sim 45°$, $d = 2 \times 15\mu$ (gelatin of Kodak 649F spectroscopic plates), and $\lambda = 500$ nm, we obtain $2\Delta\lambda_{1/2} = 10$ nm. With thicker recording material, it is possible to reduce $\Delta\lambda_{1/2}$ by a factor of 50 to 100, and thereby reduce the loss at wavelengths λ_2 close to λ_1.

B.4 EXPERIMENTAL WORK

Several dye solutions were tested: Rhodamine 6G (R6G), Na-fluorescin, 7-diethylamino-4 methylcoumarin (7D4MC), and 4-methyl-umbelliferone (4MU). The operational characteristics were similar for all dyes, and we shall confine our report to observations in an acidic solution of 4MU[6, 7] (5×10^{-3} molar 4MU + 1N $HClO_4$ in ethanol). Throughout the experiments the nitrogen laser pump pulses (337 $m\mu$) were maintained at 75 KW peak power and 8 nsec FWHM. For single line operation (G_2 blocked) the output pulses from the dye laser at 500 nm had a peak power of 10 kw and 5 nsecs FWHM. The tuning range of the laser, shown in Figure 22 was about 85 nm. The linewidth, as measured with a Fabry-Perot interferometer and averaged over 1000 pulses, was about 2 Å. By inserting a telescope with a 10X magnification into the cavity[8] between D and G_1, the linewidth was reduced to less than 0.2 Å; this resulted in a somewhat lower output power.

The results of two wavelengths operation are shown in Figure 23. G_1 was aligned for a preselected λ_1, and G_2 was adjusted to tune λ_2 over the tuning range; three representative scans are shown. For the results shown in Figures 23a and 23b, λ_1 was selected at the edges of the laser gain

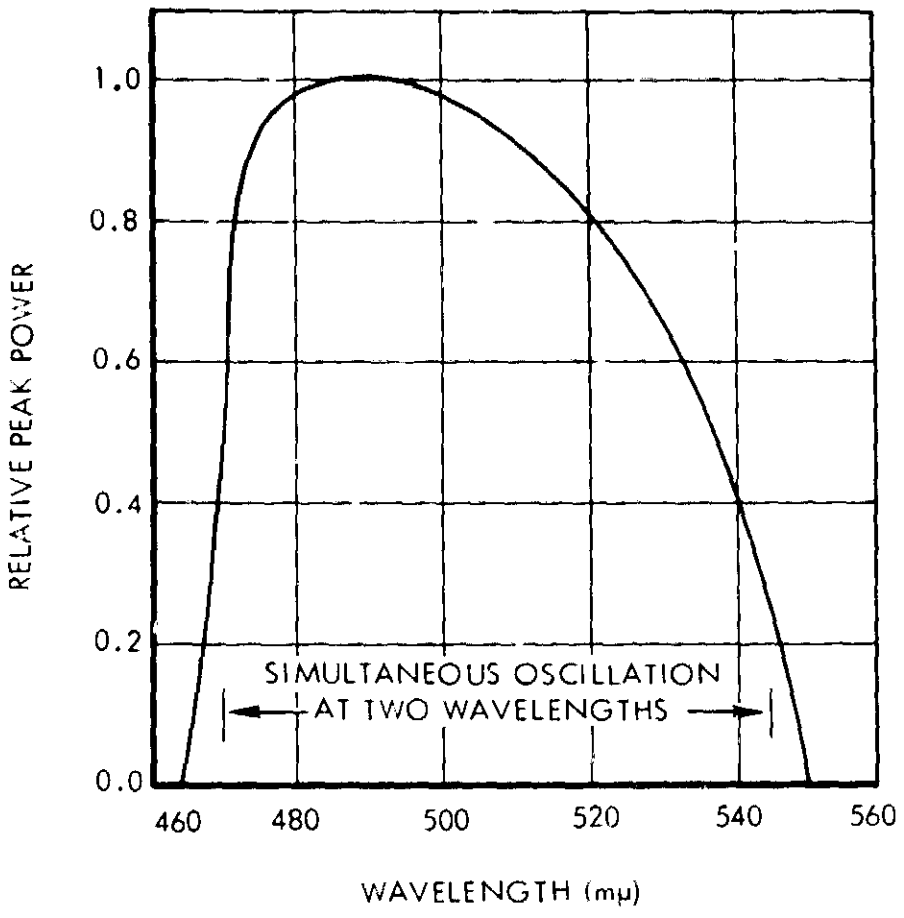

FIGURE 22. RELATIVE PEAK POWER OUTPUT AS A FUNCTION OF WAVELENGTH AT SINGLE WAVELENGTH OPERATION (5×10^{-3} MOLAR 4MU + 1N $HC10_4$ IN ETHANOL).

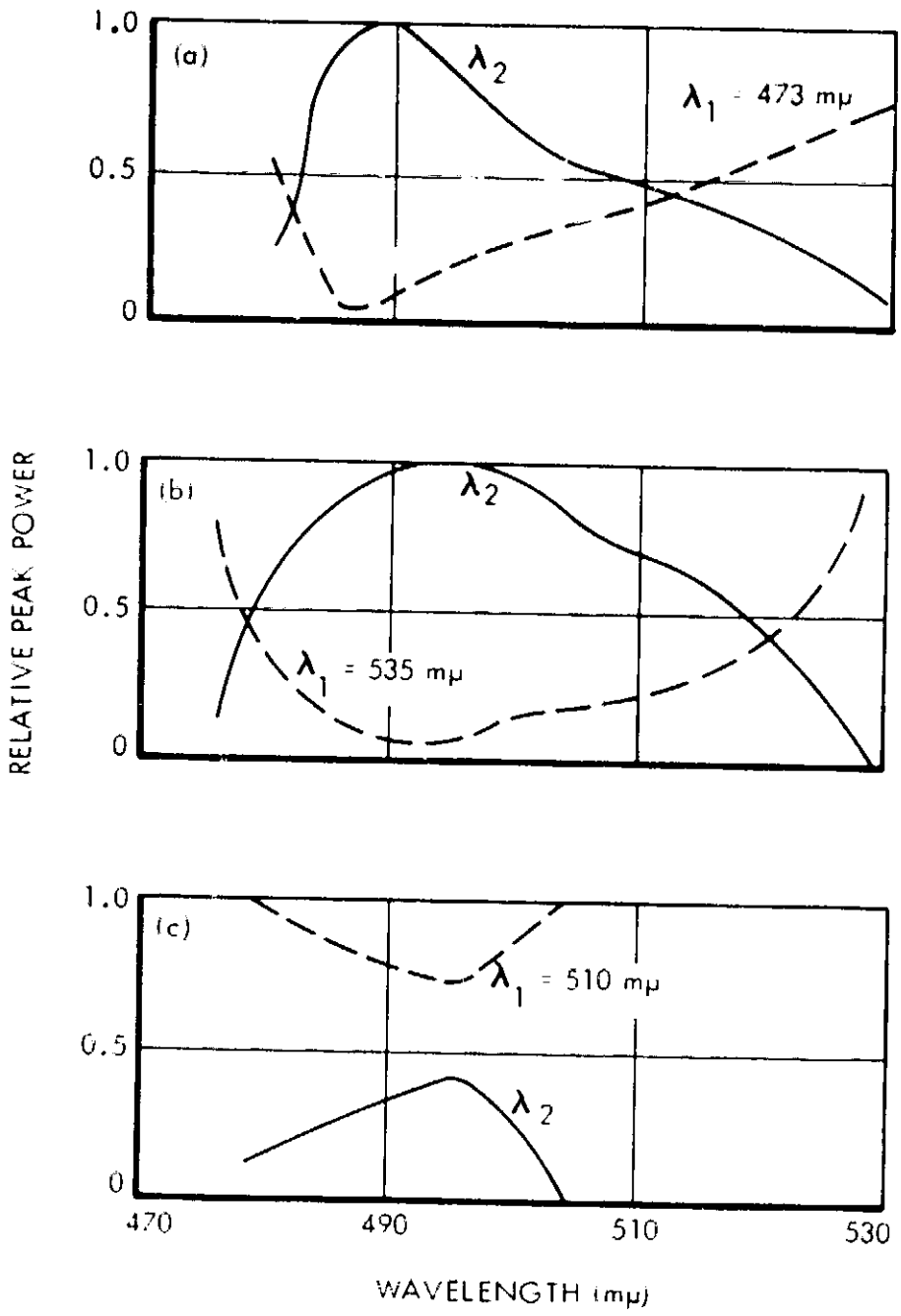

FIGURE 23. RELATIVE PEAK POWER OUTPUT AT TWO WAVELENGTHS OPERATION; λ_1 FIXED AS INDICATED AND λ_2 VARIED.

band, so the output power, for λ_2 in the central region of the gain band, is higher than the power at λ_1. However, as λ_2 approaches λ_1, the combined effect of losses due to (i) imperfect mirror reflectivity at G_1, (ii) the finite spectral bandwidth of the grating at G_1 as discussed earlier, (iii) longer cavity for λ_2, and (iv) reduction in gain, cause the power level at λ_2 to fall below the power at λ_1. A similar situation exists as λ_2 is always lower than that at λ_1, and as shown in Figure 23c, the region of simultaneous tuning is reduced. A very significant feature, demonstrated in Figure 23, is that the power at λ_1 does not remain constant as λ_2 is tuned. This behavior is expected in a homogeneously broadened medium, where the radiation fields at λ_1 and λ_2 compete, as it were, for the same inversion[9]. We note in passing that the terms homogeneous and inhomogeneous broadening must be carefully associated with the time scales involved[10]. Typical relaxation times within the excited vibration-rotation manifold are in the 10^{-12} sec range. Since the relevant times in the operation of the dye laser are in the 10^{-9} sec regime, the system can be considered to be homogeneously broadened.

To demonstrate the competition effects more clearly, we performed an experiment in which λ_1 was fixed at 537 nm (long wavelength side of the gain band) and λ_2 was fixed at 498 nm (high gain region). The power levels at λ_1 and λ_2 were monitored as various neutral density filters were inserted between G_1 and G_2. The results are shown in Figure 24. Note that for filter transmission of 1.0, the ratio between the powers at λ_2 and λ_1 is significantly higher than the same ratio at single line operation (Figure 22). This is a clear manifestation of the competition effects, showing that the high rate of stimulated emission at λ_2 reduces

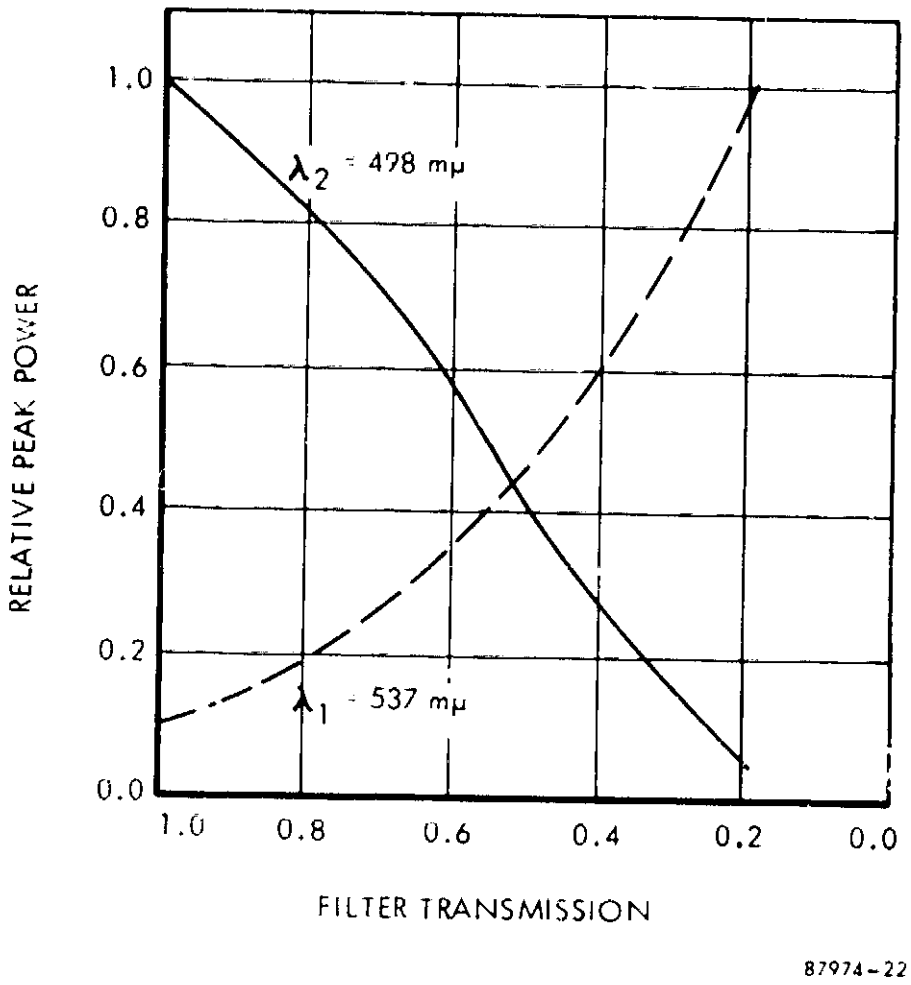

FIGURE 24. RELATIVE PEAK POWER OUTPUT, AT FIXED λ_1 AND λ_2, AS A FUNCTION OF TRANSMISSION IN THE ARM G_1 - G_2 (FIGURE 21).

the number of excited molecules available for emission at λ_1. With reduced filter transmission the power at λ_2 decreases, and the reduced rate of stimulated emission at λ_2 leaves more excited molecules available for emission at λ_1, so the power at λ_1 increases.

The detailed effects of the competition phenomena described above will differ from one experimental setup to another, depending on the losses in the cavity, mirror reflectivities, efficiencies of the gratings, the particular dye solution used, and the pump power. The basic features are, however, common to most dye systems.

In general, when aligning G_1 and G_2 for some λ_1 and λ_2, the output powers are not equal. To equalize the powers, either G_1 or G_2 can be slightly misaligned. For example, if the power at λ_1 is higher, a slight misalignment of G_1 will simultaneously reduce the power at λ_1 and increase the power at λ_2. With this technique we obtained equal powers at any chosen pair of wavelengths simultaneously, over a tuning range of 75 nm. It was possible to obtain λ_1 and λ_2 as close as 2 nm to each other. Furthermore, when the powers at λ_1 and λ_2 are equal, the pulses at both wavelengths occur simultaneously to within 0.5 nsec, and have identical shapes.

B.5 CONCLUSIONS

The method described here is versatile and can be readily extended to simultaneous operation at more than two wavelengths. For example, we achieved three wavelengths operation by introducing a third grating after G_2 and aligning it at the proper angle for some λ_3.

A two wavelength tunable pulsed laser should find many applications in spectroscopy, in contour and multicolor holography, as well as in optical mixing experiments. It could also be used conveniently for obtaining tunable infra-red radiation by difference frequency generation, which has been recently demonstrated by different groups utilizing either two lasers[11] or both signal and idler of an optical parametric oscillator[12].

B.6 ACKNOWLEDGEMENT

We are grateful to Mr. D. Pery for preparing the holographic gratings.

REFERENCES

1. D. J. Taylor, S. E. Harris, S. T. K. Nieh and T. W. Hänsch, Appl. Phys. Letters, 19, 269 (1971).

2. Edward F. Zalewski and Richard A. Keller, App. Optics, 10, 2772 (1971).

3. H. S. Pilloff, App. Phys. Letters, 21, 339 (1972).

4. H. Kogelnik, C. V. Shank, T. P. Sosnowski and A. Dienes, App. Phys. Letters, 16, 405 (1970).

5. H. Kogelnik, Bell. Sys. Tech. Jour. 48, 2909 (1969).

6. C. V. Shank, A. Dienes, A. M. Trozzolo and J. A. Myer, App. Phys. Letters, 16, 405 (1970).

7. A. Bergman, R. David and J. Jortner, Optics Comms. 4, 431 (1972).

8. T. W. Hänsch, App. Optics, 11, 895 (1972).

9. Similar effects have been observed by Pilloff; see Reference 3.

10. M. Hercher. App. Optics 6, 947 (1967).

11. C. F. Dewey and L. O. Hocker, App. Phys. Letters, 18, 58 (1971).

12. G. C. Bhar, D. C. Hanna, B. Luther-Davies and R. C. Smith, Opt. Comms., 6, 323 (1972).